Molecular Determinants of Electrical Rectification of Single Channel Conductance in Gap Junctions Formed by Connexins 26 and 32

Seunghoon Oh, Joshua B. Rubin, Michael V.L. Bennett, Vytas K. Verselis, and Thaddeus A. Bargiello

From the Department of Neuroscience, Albert Einstein College of Medicine, Bronx, New York 10461

abstract The fully open state of heterotypic gap junction channels formed by pairing cells expressing connexin 32 (Cx32) with those expressing connexin 26 (Cx26) rectifies in a way that cannot be predicted from the current–voltage (I–V) relation of either homotypic channel. Using a molecular genetic analysis, we demonstrate that charged amino acids positioned in the amino terminus (M1 and D2) and first extracellular loop (E42) are major determinants of the current–voltage relation of the fully open state of homotypic and heterotypic channels formed by Cx26 and Cx32. The observed I–V relations of wild-type and mutant channels were closely approximated by those obtained with the electrodiffusive model of Chen and Eisenberg (Chen, D., and R. Eisenberg. 1993. *Biophys. J.* 64:1405–1421), which solves the Poisson-Nernst-Plank equations in one dimension using charge distribution models inferred from the molecular analyses. The rectification of the Cx32/Cx26 heterotypic channel results from the asymmetry in the number and position of charged residues. The model required the incorporation of a partial charge located near the channel surface to approximate the linear I–V relation observed for the Cx32*Cx26E1 homotypic channel. The best candidate amino acid providing this partial charge is the conserved tryptophan residue (W3). Incorporation of the partial charge of residue W3 and the negative charge of the Cx32E41 residue into the charge profile used in the Poisson-Nernst-Plank model of homotypic Cx32 and heterotypic Cx26/Cx32 channels resulted in I–V relations that closely resembled the observed I–V relations of these channels. We further demonstrate that some channel substates rectify. We suggest that the conformational changes associated with transjunctional voltage (V_j)-dependent gating to these substates involves a narrowing of the cytoplasmic entry of the channel that increases the electrostatic effect of charges in the amino terminus. The rectification that is observed in the Cx32/Cx26 heterotypic channel is similar although less steep than that reported for some rectifying electrical synapses. We propose that a similar electrostatic mechanism, which results in rectification through the open and substates of heterotypic channels, is sufficient to explain the properties of steeply rectifying electrical synapses.

key words: gap junctions • electrical rectification • rectifying electrical synapses • Poisson-Nernst-Plank • ion channel

introduction

Heterotypic gap junctions formed by two closely related connexins (Cx),[1] Cx32 and Cx26, display marked but different asymmetries in the transjunctional voltage (V_j) dependence of initial and steady state conductances (Barrio et al., 1991; Rubin et al., 1992a; Bukauskas et al., 1995a). The reduction in the steady state conductance of Cx32/Cx26 heterotypic junctions that occurs only when the Cx26 side of the junction is depolarized relative to the Cx32 side is a consequence of the opposite gating polarity of a V_j gate found in each of the two apposed hemichannels that form the intercellular junction. Cx26 hemichannels close upon the application of relatively positive transjunctional potentials, whereas Cx32 hemichannels close upon the application of relatively negative transjunctional potentials (Verselis et al., 1994). Thus, in Cx32/Cx26 junctions one or both gates are closed by adequate positivity on the Cx26 side and neither is closed by positivity on the Cx32 side. Less is known about the mechanism underlying the V_j dependence of initial conductance in the heterotypic Cx32/Cx26 junction. The demonstration that the rectification of single channel currents of the heterotypic Cx32/Cx26 junction parallels the voltage dependence of initial conductance (Bukauskas et al., 1995a; and this paper) indicates that the underlying mechanism involves changes in ion fluxes through the open channel rather than gating.

Although considerably less steep, the rectification of initial currents observed in the heterotypic Cx32/Cx26

Dr. Rubin's current address is Joshua B. Rubin, Dana Farber Cancer Institute, Boston, MA 02115.

Address correspondence to Ted Bargiello, Department of Neuroscience, Albert Einstein College of Medicine, 1300 Morris Park Ave., Bronx, NY 10461. Fax: 718-430-8821; E-mail: bargiell@aecom.yu.edu

[1]*Abbreviations used in this paper:* CL, cytoplasmic loop; CT, COOH terminus; Cx, connexin; E, extracellular loop; I–V, current–voltage; LS channel, large diameter synthetic ion channel; NT, NH_2 terminus; PNP, Poisson-Nernst-Plank; TM, transmembrane domain.

J. Gen. Physiol. © The Rockefeller University Press • 0022-1295/99/09/339/26 $5.00
Volume 114 September 1999 339–364
http://www.jgp.org

junction qualitatively resembles that of a rectifying electrical synapse present in the abdominal nerve cord of the crayfish (Furshpan and Potter, 1959) and one found between giant fibers and motorneurons in hatchetfish (Auerbach and Bennett, 1969) that is formed by gap junction channels (Hall et al., 1985). In these electrical synapses, depolarizations but not hyperpolarizations of the presynaptic fiber produce virtually instantaneous changes in the potential of the postsynaptic fiber. Voltage clamp studies of the crayfish rectifying electrical synapse demonstrated that junctional currents elicited by presynaptic depolarization reach steady state within 800 μs and rectify extremely steeply, increasing *e*-fold per 4–5 mV of applied voltage (Giaume and Korn, 1985; Jaslove and Brink, 1986; Giaume et al., 1987).

In their original report, Furshpan and Potter (1959) hypothesized that the junctional membrane behaved as an "electrical rectifier" or diode rather than a simple electrical resistor. The separation of fixed positive and negative charges across the junctional membrane resulting from the pairing of hemichannels with opposite charges at their channel entry could form a diode (p-n junction). Mauro (1962) and Finkelstein (1963) have examined the electrical characteristics of p-n junctions formed by fixed charged membranes. The steepness of the current–voltage (I–V) relations attainable by p-n junctions provides an attractive model for the generation of steeply rectifying electrical synapses. However, Jaslove and Brink (1986) provided evidence that the crayfish rectifying synapse contains a voltage-dependent gate, as kinetic components (with a time constant of ~7.5 ms) could be resolved upon cooling the preparation to 9.5°C. They hypothesized that the steep rectification results from a structurally asymmetric junction, in which one hemichannel contains a "fast" voltage-dependent gate that closes upon depolarization of the presynaptic element. However, a substantial fast kinetic component remained in the cooled preparation. This result suggests that an additional process, unrelated to voltage-dependent gating, may also be involved. Giaume et al. (1987) also suggested that the crayfish synapse was structurally asymmetric and suggested that the steep rectification was a consequence of a highly voltage-dependent probability of opening of one of the hemichannels that forms the rectifying synapse.

The connexins forming rectifying electrical synapses in vertebrates and invertebrates have not yet been identified and indeed the invertebrate gap junctions are formed by proteins encoded by another gene family with no primary sequence homology to the vertebrate connexin gene family (Phelan et al., 1998). Although the rectification observed for Cx32/Cx26 heterotypic junctions is much less steep than that observed in rectifying synapses, the elucidation of the molecular determinants underlying the rectification of initial conductance in these channels may shed light on the mechanism governing the rectification of electrical synapses.

The results of the molecular genetic studies described in this paper demonstrate that charged amino acid residues located in the amino terminus and first extracellular loop are major determinants of the rectification of the heterotypic Cx32/Cx26 channel. The rectifying I–V relation of the heterotypic channel results from a structural asymmetry arising from differences in the number and position of fixed charges present in the Cx32 and Cx26 hemichannels. The different I–V relations of homotypic channels can be explained by the different symmetrical charge distributions that result from homotypic pairings. Furthermore, we show that homotypic and heterotypic channels can enter substates that rectify. The nonlinearity of the I–V relations of these substates is likely to result from the increased electrostatic effect of charged residues present in the amino terminus of one hemichannel that arises from a conformational change associated with V_j-dependent gating. This finding suggests that the change in conductance resulting from V_j gating may correspond to a narrowing of the entry of the connexin hemichannel near the cytoplasmic surface. We suggest that the rectification of single channel currents like that observed in the fully open state and substates of gap junction channels is responsible for the steep and rapid rectification observed in some electrical synapses.

materials and methods

Construction of Chimeric Connexins, Site-directed Mutagenesis, RNA Synthesis, and Oocyte Injection

Chimeras of Cx26 and Cx32 were constructed by the procedure described by Rubin et al. (1992a) or, when possible, by using restriction enzyme sites that are conserved among connexins and chimeric constructs. In this study, we define for Cx26: the NH_2 terminus (NT) as containing amino acids 1–22 inclusively, the first transmembrane domain (TM1) amino acids 23–40, the first extracellular loop (E1) amino acids 41–75, the second transmembrane domain (TM2) amino acids 76–93, the cytoplasmic loop (CL) amino acids 94–131, the third transmembrane domain (TM3) amino acids 132–151, the second extracellular loop (E2) amino acids 152–189, the fourth transmembrane domain (TM4) amino acids 190–209, and the COOH terminus (CT) amino acids 210–226. Cx32 has one fewer amino acid in the CL domain than does Cx26. Consequently, CL of Cx32 consists of amino acids 94–130, TM3 amino acids 131–150, E2 amino acids 151–188, TM4 amino acids 189–208, and CT amino acids 209–283. In our notation, a chimera designated as Cx32*Cx26E1 has the sequence of the E1 domain of Cx32 replaced with that of Cx26. In a chimera designated as Cx32*Cx26($NT_{1–11}$ + CL), the first 11 amino acids of the NH_2 terminus of Cx32 are replaced with the first 11 amino acids of the NH_2 terminus of Cx26 and the CL domain of Cx32 is replaced with the CL domain of Cx26. A chimera designated as Cx32*Cx26(CL–CT) would have the entire region spanning the cytoplasmic loop through the COOH

terminus of Cx32 (amino acids 94–283) replaced with the equivalent region of Cx26 (amino acids 94–226).

Site-directed point mutations were constructed using oligonucleotide primers and the polymerase chain reaction. All chimeric constructs and point mutations were cloned into the plasmid vector, pGEM-7zf (+) (Promega Corp.) and sequenced in entirety. RNA was transcribed in vitro from linearized plasmid templates as described in Rubin et al. (1992a). For oocyte expression of cloned connexins, approximately 50 ηl of 1 ηg/ηl RNA was coinjected with 0.3 ρmol/ηl of an antisense phosphorothioate oligonucleotide complimentary to *Xenopus* Cx38. This antisense oligonucleotide blocks all endogenous coupling between oocyte pairs attributable to Cx38 within 72 h (Barrio et al., 1991; Rubin et al., 1992a,b).

Electrophysiological Recording of Xenopus Oocyte Pairs

Oocytes were devitellinized and paired 12–24 h after RNA injection. Expression of junctional currents usually developed within 4 h of pairing. Only cells expressing <5 μS junctional conductance were employed to minimize the effects of access resistance on voltage dependence (Jongsma et al., 1991; Rubin, 1992). Recordings were obtained with a dual voltage clamp with glass electrodes containing 1 M KCL solutions. Pipette resistance was ~5 MΩ. Coupled oocytes had equal resting membrane potentials that varied between −30 and −60 mV. Cells were voltage clamped to their resting potential (0 mV transjunctional voltage) and a family of junctional currents for each cell pair was generated by applying transjunctional voltages of ±5–125 mV in an ascending series of 5-mV increments. Total pulse length was 20 s with a 90-s interpulse interval. Currents were digitized at two rates, first at 256 Hz for 2 s, and then at 28 Hz for the remainder of the trace. This allowed for greater accuracy in the measurement of initial currents while not requiring the collection of an excessive number of points during the extended time necessary for junctional currents to reach steady state. Each transjunctional voltage step was preceded by a 10-mV prepulse of short duration (100–500 ms) that was used to normalize junctional currents within a family of current traces. In heterotypic junctions, current traces were scaled independently to prepulses of appropriate polarity of V_j since the prepulse amplitude elicited by a hyperpolarizing prepulse would not be the same as for a depolarizing prepulse administered to the same cell. Initial and steady state currents were determined by extrapolation of exponential fits to $t = 0$ and $t = \infty$. Initial (g_0), steady state (g_∞), and residual (g_{min}) conductances were normalized to the value of initial conductance, g_0 at $V_j = 0$ to obtain G_0, G_∞, and G_{min}. Additional details are provided in Rubin et al. (1992a,b) and Verselis et al. (1994).

Cell Transfections

The coding regions of wild-type and mutant connexins were cloned into pCI-neo (CMV promoter) vector (Promega Corp.) and transfected into the mouse *Neuro-2a* cell line and a second *Neuro-2a* cell line that expressed green fluorescent protein (GFP). Heterotypic channels were formed by mixing cell lines expressing different connexins, in which one member of the cell pair could be identified by the presence of GFP. In some cases, GFP expression was linked to that of a given connexin by the presence of an internal ribosomal entry site (IRES) sequence provided by H.-S. Shin (POSTECH, Pohang, South Korea). Transfected cell lines expressing exogenous connexins but not Cx45, which forms endogenous channels in *Neuro-2a* cell lines, were selected for single channel analysis. Cx45 channels are easily distinguished by their single channel conductance (~30 pS slope conductance), lack of substantial residual conductance states, and steep voltage dependence.

Electrophysiological Recordings of Transfected Neuro-2a Cell Pairs

Single channel and macroscopic (10–20 channels) records of gap junctions channels were obtained using double whole cell patch recordings (Neyton and Trautman, 1985) as described in Oh et al. (1997). Cells were held at 0 mV, their resting potential in the recording solutions used. Unless otherwise specified, data were acquired using pCLAMP 6.0 software, filtered at 1 kHz with a four-pole low pass Bessel filter and digitized at 5 kHz using Axopatch 200B integrating patch amplifiers and a Digidata 1200A interface (Axon Instruments). Pipette resistances were 5–10 MΩ. All points histograms were constructed with a bin size of 0.05 pA and fit to a Gaussian using Origin 4.0 software (Microcal Software Inc.).

Poisson-Nernst-Plank Model

The Poisson-Nernst-Plank (PNP) model used is that of Chen and Eisenberg (1993). Computer programs used to solve the PNP equations were downloaded from http://144.74.27.66/pnp.html. Additional details are provided in the discussion.

results

voltage dependence of homotypic and heterotypic junctions formed by Cx32 and Cx26

Macroscopic Currents Obtained from Pairs of Xenopus Oocytes

Conductance–voltage relations and representative current traces of homotypic Cx32, Cx26, and heterotypic Cx32/Cx26 gap junctions expressed in pairs of *Xenopus* oocytes are shown in Fig. 1. Both the initial and steady state conductance–voltage relations of homotypic gap junctions formed by Cx32 are symmetric about $V_j = 0$ (Fig. 1 A). Initial conductance (▼) is maximal at $V_j = 0$ and reduced by ~30% at large transjunctional voltages. At large transjunctional voltages, the steady state conductance–voltage relation decreases to a minimal conductance, G_{min}, of ~0.3. In Cx26 homotypic junctions (Fig. 1 B), initial conductance displays some dependence on the absolute voltage difference between the inside and outside of the cells (termed V_m or V_{i-o}), detected as asymmetry between the effects of depolarizing one cell and hyperpolarizing the other to the same extent (Barrio et al., 1991; Rubin et al., 1992a,b). Junctional currents relax slowly for either polarity of V_j and conductance decreases to a minimum at higher transjunctional voltages, corresponding to a G_{min} of ~0.2 at positive transjunctional voltages. There is a small asymmetry in the steady state conductance–voltage relation depending on whether one cell is hyperpolarized or depolarized. As reported previously (Barrio et al., 1991; Rubin et al., 1992b), heterotypic junctions formed by Cx32 and Cx26 are characterized by an asymmetric conductance–voltage relation (Fig. 1 C) that depends only on V_j. The rectification of initial currents results in an increase in conductance when the cell expressing Cx26 is made relatively positive and a decrease in con-

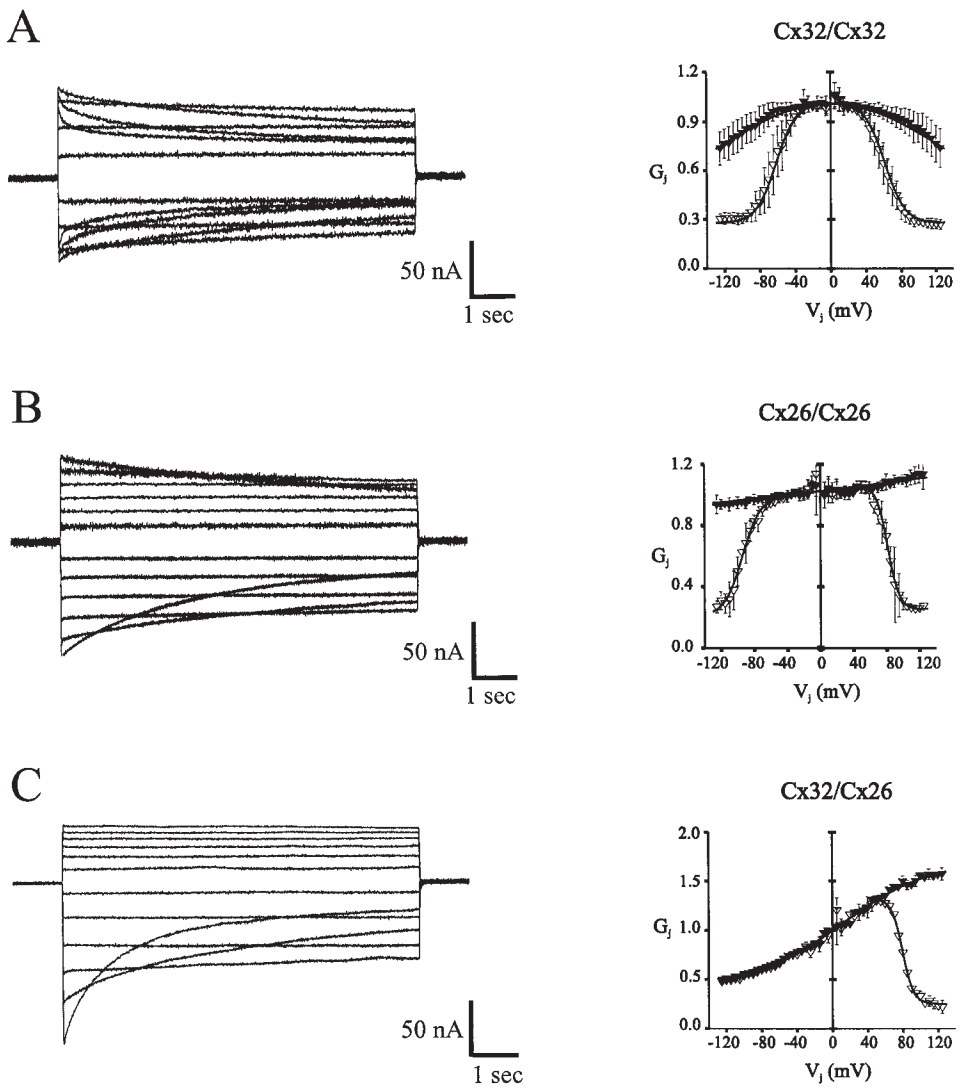

Figure 1. Conductance–voltage relations and representative traces of initial and steady state junctional currents obtained in pairs of *Xenopus* oocytes. (A) Cx32 homotypic junctions. (B) Cx26 homotypic junctions. (C) Cx32/Cx26 heterotypic junctions. Initial conductance is depicted by ▼, and steady-state conductance by ▽. In all cases, positive V_j is relative positivity at the cytoplasmic mouth of the hemichannel appearing on the right side of the channel designation. For example, in the heterotypic junction, the x axis gives the V_j of the Cx26 side of the junction. The conductance–voltage relations of each junction are the average of at least 10 separate oocyte pairs.

ductance when this cell is made relatively negative. Typically, initial conductance is approximately three times greater when the Cx26-expressing cell is stepped to $V_j = +120$ mV than when it is stepped to $V_j = -120$ mV. The steady state conductance normalized to the initial conductance (Fig. 1 C, ▽) decreases only when the Cx26 side of the heterotypic junction is stepped to positive transjunctional potentials exceeding 40 mV. G_{min}/G_0 is ~0.2.

Single-Channel Recordings of Cx26 and Cx32 in Transfected Neuro-2a Cell Lines

Homotypic Cx32 channels. A record of a homotypic rat Cx32 single channel between *Neuro-2a* cells is shown in Fig. 2. The single channel properties of rat Cx32 are similar to those that we have reported for human Cx32 (Oh et al., 1997). The primary sequence of rat and human Cx32 differ by only four amino acid residues. In the segments of the single channel records shown in Fig. 2, A and B, V_j steps of ±60 mV were applied from a holding potential of 0 mV by polarizing one member of the cell pair at the times denoted by the numeral 1 in the figure. The changes in current, recorded from the unstepped cell, correspond to a junctional conductance of ~68 pS in both cases, which we ascribe to the conductance of the fully open channel.

The boxed portion of the record shown in Fig. 2 A (expanded in Fig. 2 C) illustrates the presence of three different subconductances in rat Cx32 homotypic junctions: ~26 pS (S1), ~19 pS (S2), and ~10 pS (S3), determined from the all points histogram shown in Fig. 2 D. We believe that these subconductances correspond to at least three distinct subconductance states of rat Cx32 homotypic channels (see also Oh et al., 1997). The average conductance, determined from an all-points histogram of the entire trace (data not shown), is ~20 pS, a value that corresponds to a 75% reduction

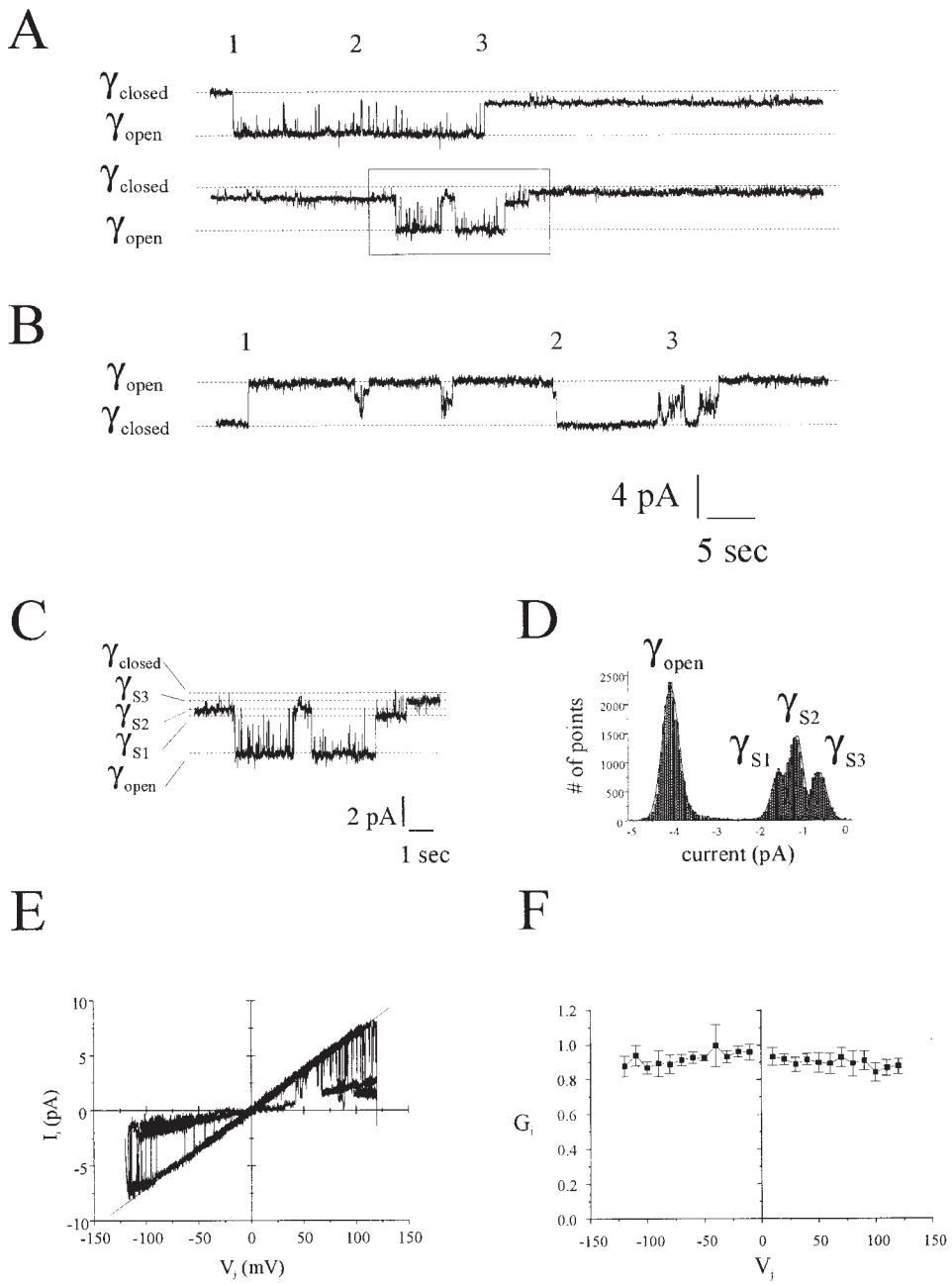

Figure 2. Single channel records of rat homotypic Cx32 expressed in pairs of *Neuro-2a* cells. (A) A segment of a continuous record of junctional currents elicited by a V_j of +60 mV applied at position 1 in the record. Numerals 2 and 3 illustrate brief and long lived closing to a substate (see text). The trace shown was digitally filtered at 250 Hz for presentation. (B) A segment of the same single channel record shown in A, but after the application of V_j of −60 mV at position 1. All gating transitions shown in this record correspond to "loop gating" events (see text). In other records, V_j-dependent gating transitions to substates comparable to that shown in A predominate. The trace shown was digitally filtered at 250 Hz for presentation. (C) The boxed segment of the trace shown in A is expanded to show the presence of at least three residual states: S1, S2, and S3. (D) An all-points histogram of the trace shown in C, illustrating transitions from the open state to residual conductance states of 26 (S1), 19 (S2), and 10 (S3) pS. The conductance of the fully open state is 68 pS. (E) I–V relation of Cx32 single channel resulting from the superimposition of 10 sequential voltage ramps of 6-s duration over ±120 mV. The straight line corresponds to a linear fit of the traces over the range of ±50 mV. Individual traces were digitally filtered at 100 Hz for presentation. (F) The conductance–voltage relation of initial currents averaged and normalized to the maximal conductance from 10 pairs of *Neuro-2a* cells expressing 15–20 intercellular Cx32 channels. Error bars represent standard deviation at each V_j.

in the conductance of the fully open state. This value is comparable to the G_{min}/G_0 of 0.3 observed in macroscopic recordings of Cx32. This suggests that the voltage-dependent entry of the channel into one of several possible subconductance states is a major determinant of the residual conductance observed macroscopically at large transjunctional voltages (see also Bukauskas and Weingart, 1994; Moreno et al., 1994).

Cx32 channels can also display gating that involves a complex series of transitions between fully open and fully closed states (Fig. 2 B, positions 2 and 3; see also Oh et al., 1997). Although not demonstrated in this record, complete closure of the rat Cx32 channel by these transitions can occur from either the fully open state or the subconductance states. This gating is similar in appearance to the slow gating during block by CO_2 and recovery (Bukauskas and Peracchia, 1997), the ionic currents expressed during channel formation, termed "docking or formation currents" by Bukauskas et al. (1995b), and to the transitions between fully closed and open states in Cx46 hemichannels, termed "loop gating" by Trexler et al. (1996).

Trexler et al. (1996) suggested that "loop gating" involves a series of conformational changes involving the extracellular loops of the Cx46 hemichannel. In contrast, V_j-dependent gating involves conformational changes that result in the entry of the channel into one of several possible discrete subconductance states. Bukauskas and Weingart (1994) have noted the similarity of the complex transitions observed in vertebrate intercellular channels to V_m gating observed in insect gap junctions. The partial closures of the channel observed between positions 1 and 2 in Fig. 2 B likely correspond to loop gating transitions that did not result in complete channel closure.

The record also is suggestive of additional complexities in V_j-dependent gating. Homotypic rat Cx32 channels appear to be able to enter into either long- or short-lived subconductance states. For example, at the beginning of the trace shown in Fig. 2 A, the channel flickered extensively, often entering a residual conductance state for <100 ms (exemplified by the transitions at position 2). In contrast, at position 3, the channel entered a 19-pS state that lasted 30 s and, later in the record, the channel entered a 10-pS state from which it had not exited when the V_j step was terminated 20 s later. In other records, we have observed that a Cx32 homotypic channel can remain in a residual conductance state for several minutes (data not shown). The presence of short- and long-lived subconductance states is also evident in the records shown in Figs. 2 E and 3.

Fig. 2 E shows that the I–V relation of the fully open state of a single Cx32 channel is nearly linear, although currents do decrease slightly, by ~5%, for either polarity of large transjunctional voltages. A similar deviation from linearity is also observed in the conductance–voltage relations of initial currents of Cx32 recorded macroscopically in *Neuro-2a* cell lines that are expressing 15–20 intercellular channels (Fig. 2 F).

Fig. 3 illustrates the gating and I–V relations of Cx32 subconductance states as well as the fully open state. When the channel resided in the fully open state, the application of a 500-ms voltage ramp from −100 to + 100 mV (Fig. 3 C) elicited a junctional current (Fig. 3 A) that only slightly deviates from linearity. However, when the channel resided in a long-lived subconductance state, the application of the same voltage ramp resulted in a nonlinear change in junctional current (Fig. 3 B). In this case, chord conductance decreased approximately twofold as the V_j ramp became more positive (from 2.4 pA at −100 mV to 1.2 pA at +100 mV). The return of junctional current to the same level (2.4 pA) as measured before the application of the voltage ramp makes it unlikely that the nonlinearity of junctional currents resulted from gating transitions between different subconductance states that could not be resolved in the record. Furthermore, reversing the time course of the voltage ramp (from +100 to −100 mV) while the channel resided in the same subconductance state reversed the time course of the rectification; junctional current now increased (from 1.2 to 2.0 pA) as the voltage ramp became more negative (not shown). Based on the negative V_j gating polarity of hemichannels formed by Cx32 (Verselis et al., 1994), it is likely that the negative voltage step (Fig. 3 C) caused the closure of the hemichannel in the stepped cell.

Fig. 3 D illustrates the rectification observed in another cell pair using a similar test paradigm but starting from an initial voltage step of +100 mV and applying a voltage ramp of shorter duration (100 ms). Unlike the previous example, the application of a positive voltage to the stepped cell is expected to cause closure of the V_j gate in the hemichannel present in the unstepped member of the cell pair. In this case, junctional currents decreased nonlinearly as the voltage was ramped from +100 to −100 mV. The difference in the direction of rectification in these two cases is a consequence of the closure of opposite hemichannels. In the former case (Fig. 3 B), it is likely that the V_j gate in the hemichannel in the stepped cell closed, whereas in the second case (Fig. 3 D), it is likely that the V_j gate in the hemichannel in the unstepped cell closed.

In other instances, we have observed that the I–V relations for other Cx32 substates do not rectify appreciably (data not shown). Thus, it appears that Cx32 hemichannels may adopt several different closed conformations. Although we have not examined the I–V relations of all substates extensively, the available data suggest that the longer lasting substates rectify.

The linearity of the I–V relation of the fully open Cx32 channel differs from expectation based on the 30% reduction in initial conductance observed for Cx32 homotypic junctions formed between pairs of *Xenopus* oocytes. Differential modification of the protein subunits or the presence of ancillary proteins in one of the two expression systems is unlikely to cause the different behavior of the initial currents, because initial currents in Cx26/Cx32 heterotypic junctions are almost identical in oocytes and transfected *Neuro-2a* cell lines (see Figs. 1 C and 5 F). A possible explanation, described in the discussion, is that the rectification observed in oocytes arises from the difference in the intracellular ion composition of the two experimental systems. The concentration of permeable anions should be less in oocyte cell pairs than in *Neuro-2a* cells dialyzed with CsCl patch recording solutions.

Homotypic Cx26 channels. A record of a single homotypic Cx26 channel between *Neuro-2a* cells is shown in Fig. 4 A. Initially, the cells appeared to be uncoupled, as the application of a +60-mV voltage step to one member of the cell pair (Fig. 4 A, position 1) did not change the current measured in the unstepped cell.

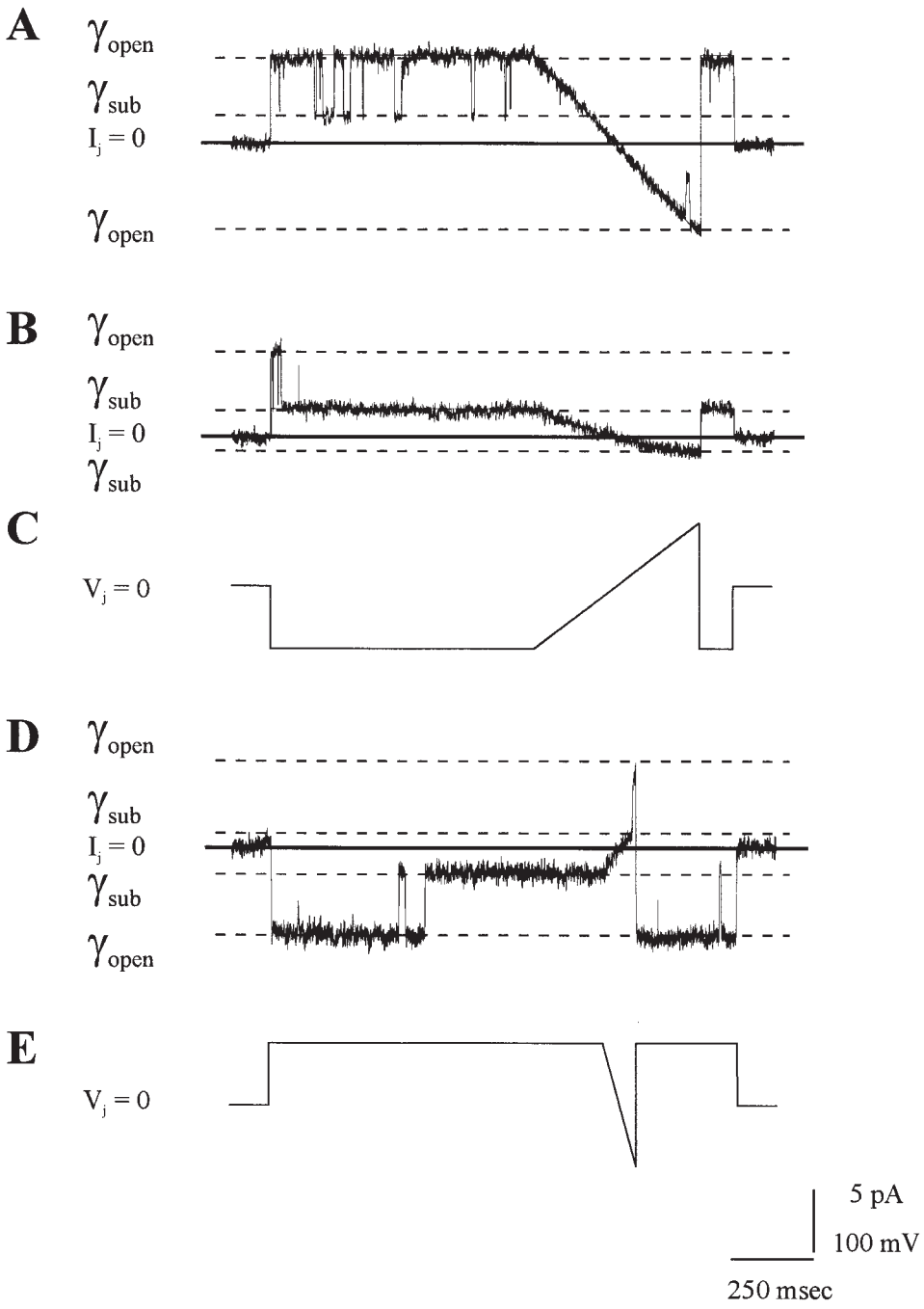

Figure 3. Rectification of ionic currents through Cx32 substates. (A) A current trace of a single Cx32 homotypic channel resulting from the experimental paradigm shown in C. After an initial transjunctional voltage step of −100 mV, the transjunctional voltage was ramped to +100 mV in 500 ms, and then stepped back to the original holding potential (−100 mV). In A, the channel resided in the fully open state for the duration of the voltage ramp and the resulting I–V relation deviates slightly from linearity. (B) A subsequent trace obtained from the same cell pair in which the channel entered into a long-lived substate. In this case, currents rectify, decreasing nonlinearly as the transjunctional voltage becomes more positive. (D) A current trace from a Cx32 homotypic channel elicited by the experimental paradigm shown in E. In this case, an initial transjunctional voltage of +100 mV was applied and subsequently ramped to −100 mV in 100 ms. The entry of the channel into a subconductance state results in a nonlinear I–V relation, such that the junctional conductance decreases as the transjunctional voltage becomes negative. Data were acquired with a sampling frequency of 5 kHz and filtered a 1 kHz with a four-pole Bessel filter. The current traces were digitally filtered at 200 Hz for presentation.

The channel opened subsequently via a series of complex, poorly resolved events that resemble "loop gating" or "docking/formation currents." In the segment of the trace shown in Fig. 4 B, (and expanded in Fig. 4 C), the channel opened and closed by a similar series of complex gating events while a V_j of −60 mV was applied. In the record shown, the conductance of the fully open channel is 130 pS. In other records, we have observed the conductance of the fully open Cx26 channel to be ~150 pS at ±60 mV. There was a single V_j-dependent gating event (Fig. 4 A, position 2) corresponding to a 104-pS transition that resulted in a 26-pS residual conductance state (substate). The residual conductance, ~20% of the fully open state, is in agreement with the G_{min}/G_0 of ~0.2 that is observed in macroscopic recordings. The relatively few gating transitions observed at ±60 mV is consistent with that expected, given a $V_{1/2}$ of ~90 mV determined from the macroscopic conductance–voltage relation shown in Fig. 1 B. The channel shows more gating at higher transjunctional voltages (±120 mV). It is likely that homotypic Cx26 channels may also enter into one or more substates with residual

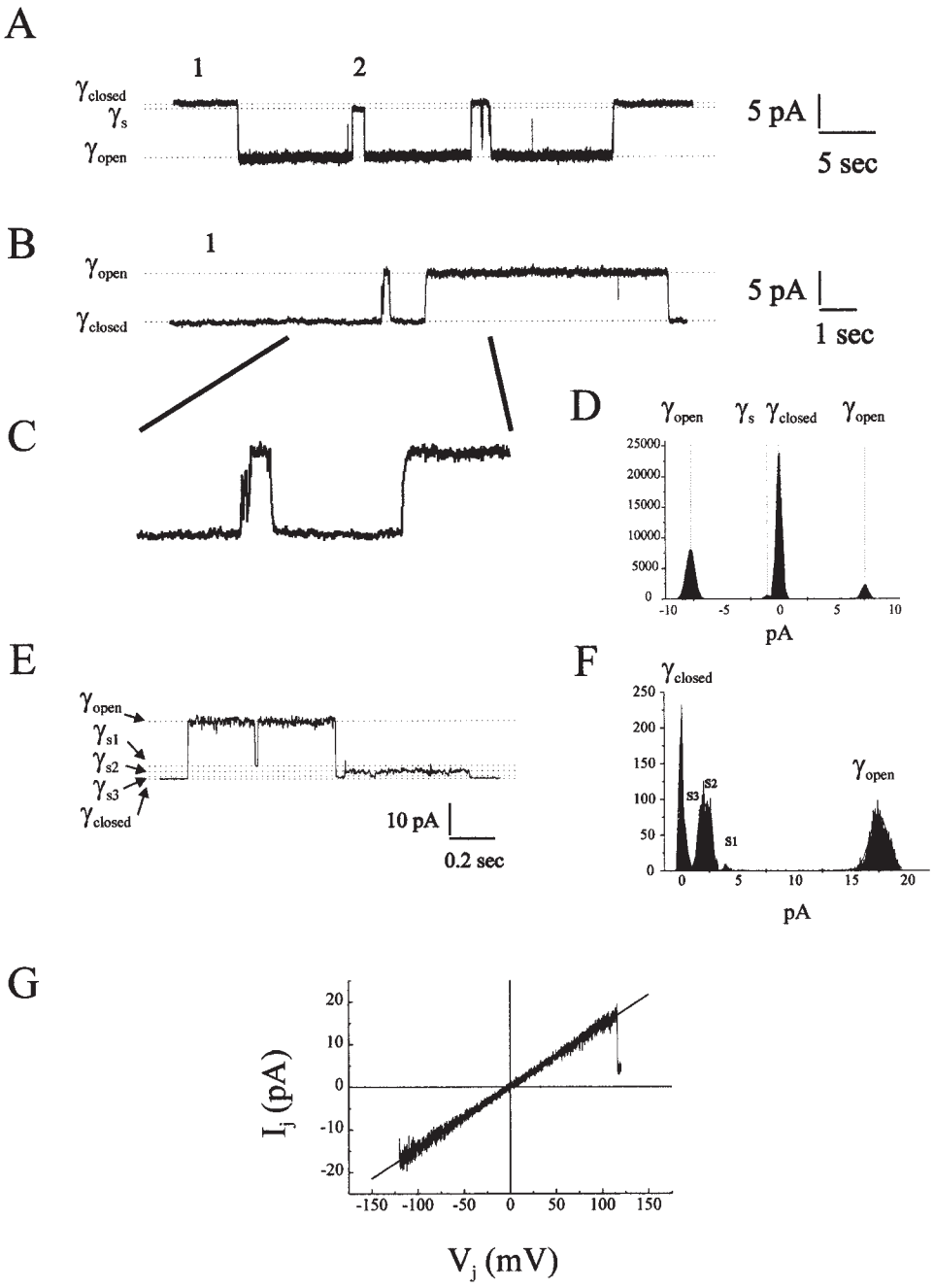

Figure 4. Single channel records of rat homotypic Cx26 gap junctions expressed in pairs of *Neuro-2a* cells. (A) A segment of a continuous recording of a single Cx26 homotypic channel at V_j of +60 mV. (B) A segment of a recording of the same cell pair at a V_j of −60 mV. (C) The segment of the trace shown in B is expanded to show "loop gating" transitions. (D) All points histogram of the traces in A and B showing substate and fully open states. (E) A segment of a single homotypic Cx26 channel record at V_j = −120 mV. (F) All points histogram of the trace shown in E. The conductance of the fully open state is ~140 pS. The conductances of the residual conductance states are: S1 ~ 30 pS, S2 ~ 20 pS, and S3 ~ 15 pS. (G) I–V relation of the open state of Cx26 channel obtained by applying a 6-s voltage ramp over ±120 mV. Records shown in A–C and G were digitally filtered at 300 Hz for presentation, record in E at 100 Hz.

conductances lying between 10 and 30 pS, as shown in the current trace (Fig. 4 E) and all points histogram (Fig. 4 F). Cx26 junctional currents characteristically appear noisier when the channel resides in a high conductance state than when it resides in either a subconductance or the fully closed state. This suggests the existence of multiple open states whose average conductance is ~130–150 pS.

The I–V relation of the open state of Cx26 homotypic channels is linear (Fig. 4 G). In contrast to the expression of Cx26 in oocytes, there does not appear to be any dependence on V_m in Cx26-transfected cell lines, as the I–V relation is symmetric at $V_j = 0$ over a ±120-mV ramp. The insensitivity of Cx26 hemichannels to V_j ($V_{1/2}$ = ±90 mV) and the rapid opening of Cx26 hemichannels upon stepping to smaller transjunctional voltages (not shown) precluded the examination of the I–V relation of Cx26 substates.

Heterotypic Cx32/Cx26 channels. A record of a heterotypic Cx32/Cx26 channel between *Neuro-2a* cells is shown in Fig. 5. Both cells were initially held at 0 mV. At position 1 in the trace shown in Fig. 5 A, the cell expressing Cx32 was stepped to −80 mV, eliciting a junctional current corresponding to a conductance of 120

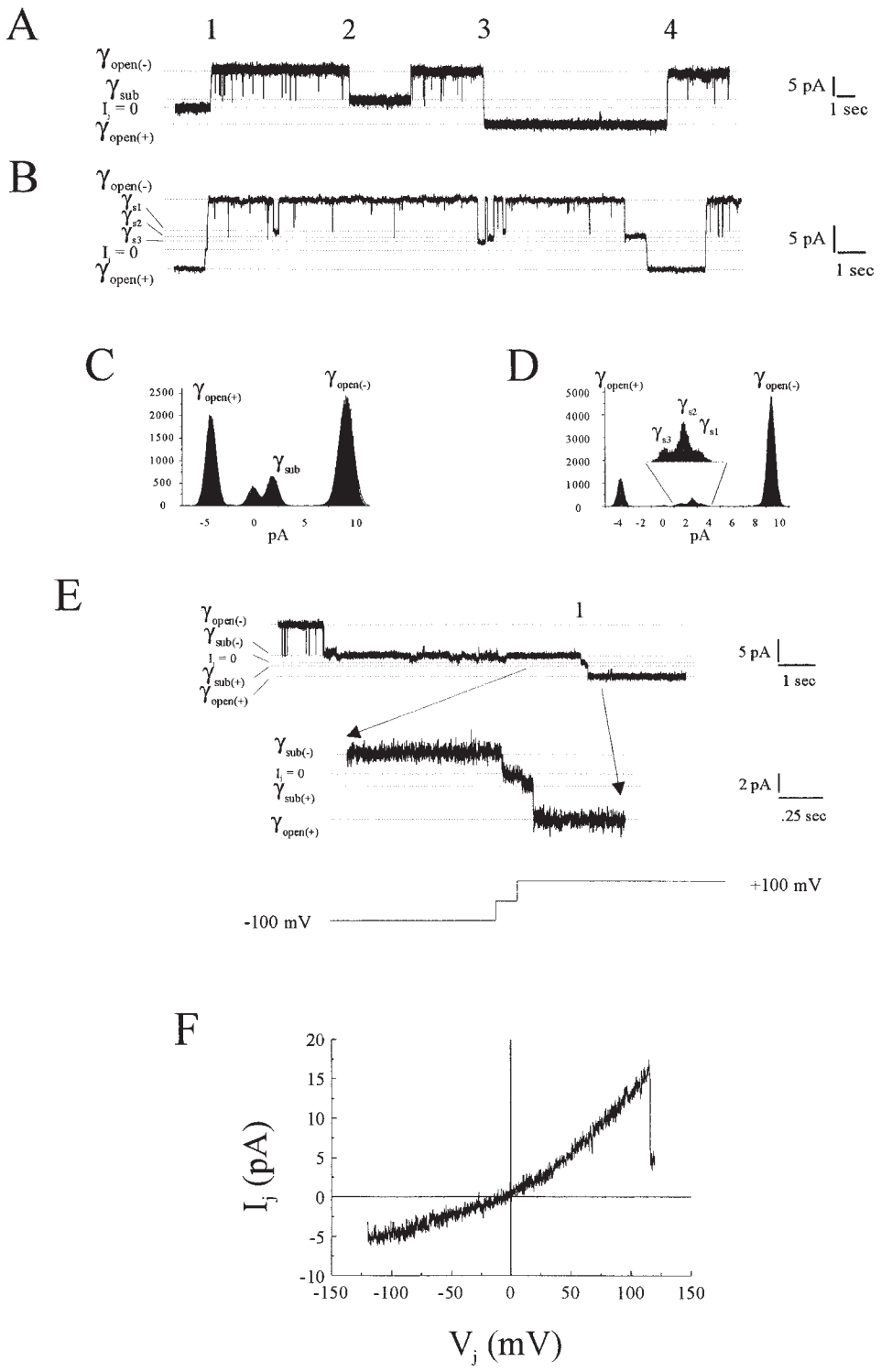

Figure 5. Single channel records of heterotypic Cx32/Cx26 channels expressed in pairs of *Neuro-2a* cells. (A) In this record, a −80 mV transjunctional voltage was applied at position 1 by stepping the cell expressing Cx32 from an initial holding potential of 0 mV. At position 2, the intercellular channel entered a residual conductance state and at position 3 the polarity of V_j was reversed to +80 mV and reversed again to −80 mV at position 4 (see text for details). The record was digitally filtered at 500 Hz for presentation. (B) In this record, the Cx32 cell was sequentially hyperpolarized and depolarized resulting in the following sequence of transjunctional voltages: + 80 to 0 mV (briefly), to −80 to 0 to +80 mV, and finally to −80 mV. This trace illustrates the presence of three subconductance states that occur when the cell expressing the Cx26 side of the junction is relatively positive (negative with respect to the Cx32-expressing cell). The record was digitally filtered at 200 Hz for presentation. (C) The all-points histogram of the trace shown in A (see text for details). (D) The all-points histogram of the trace shown in B (see text for details). (E) In this record, a transjunctional voltage of −100 mV was applied by hyperpolarizing the cell expressing Cx32. At position 1, the channel had closed to a subconductance state, at which time V_j was returned briefly to zero, and then to +100 mV. The record was digitally filtered at 500 Hz for presentation. (F) The I–V relation of an open Cx32/Cx26 heterotypic channel obtained by applying a 6-s voltage ramp over ±120 mV. Positive V_j is positivity on the Cx26 side of the channel. The record was digitally filtered at 200 Hz for presentation.

pS (Fig. 5 C). At position 2, the channel underwent an ~95-pS transition, which resulted in an ~25-pS subconductance state. The trace presented in Fig. 5 B and the corresponding all points histogram (Fig. 5 D) demonstrates the existence of at least three additional substates of ~20, 30, and 40 pS in the heterotypic channel. We ascribe these transitions to subconductance states resulting from V_j-dependent gating that could have occurred if either the V_j gate in the Cx32 or the Cx26 hemichannel or both gates had closed. Recall that the polarity of V_j-dependent gating is opposite in the two hemichannels with Cx32 closing for relatively negative V_j at its cytoplasmic face and with Cx26 closing for relatively positive V_j.

The rectification of ionic currents through the fully open heterotypic channel is shown in Fig. 5, A and F. In Fig. 5 A, the voltage was stepped from −80 to +80 mV at position 3. The conductance of the fully open channel was ~2.5-fold greater at −80 (120 pS) than at +80 (50 pS) mV, (Fig. 5 C). Fig. 5 F shows the I–V relation obtained by applying a ±120-mV ramp to the cell pair expressing Cx26. In this record, single channel currents rectify approximately threefold over the ±120 mV range.

Rectification of the same polarity was also observed in a substate of the heterotypic channels. In Fig. 5 E, position 1, the voltage was stepped briefly from −100 to 0 mV, and then to +100 mV, but in this case the polarity of the V_j step was reversed while the channel resided in a 25-pS substate. The channel remained in this substate briefly before transiting to the fully open state. The conductance of the substate at +100 mV was 9.5 pS, compared with 25 pS at −100 mV, corresponding to a rectification of ~2.5-fold. The degree and polarity of rectification of this substate is similar to that observed for the rectification of the fully open state in this record (125–45 pS or 2.8-fold at comparable voltages).

We observed discrete gating transitions (V_j dependent) from the fully open state when the Cx26-containing cell was depolarized or the Cx32-expressing cell was hyperpolarized. This result is consistent with the observed relaxation of steady state currents in macroscopic recordings of Cx32/Cx26 heterotypic junctions. On occasion, we observe complete channel closure via "loop gating" during the application of either polarity of V_j in this heterotypic junction (data not shown), which supports the hypothesis that this gating occurs by a mechanism distinct from V_j-dependent gating. If the "loop gate" is weakly voltage dependent, then this observation could explain the slight difference in the initial and steady state conductance–voltage relations that is observed in macroscopic records of some heterotypic junctions at polarities of transjunctional voltage that should not close the V_j gate. For example, there is a decrease in steady state junctional conductance at negative V_j in the conductance–voltage relations in Fig. 6, A and B.

molecular determinants of the voltage dependence of initial currents

As a means of establishing the mechanism underlying the rectification of junctional currents, we sought to localize the molecular determinants of the process. Our approach can be summarized by the following question: What amino acid residues in Cx26 and Cx32 must be exchanged to interconvert their I–V relations in heterotypic as well as homotypic junctions?

The difference in the gating polarity of the steady state V_j dependence of Cx32 and Cx26 hemichannels is due to a single amino acid difference in the sequence of the NH_2 terminus of these two connexins (Verselis et al., 1994). The replacement of the neutral asparagine residue (N2) normally present in Cx32 with the negatively charged aspartate residue (D2) found in wild-type Cx26 reverses the V_j gating polarity of Cx32 hemichannels. Similarly, the reciprocal substitution (Cx26D2N) reverses the gating polarity of Cx26, from closure on relatively positive V_j to closure on relatively negative V_j. We proposed that amino acid residues at this position form a vestibule for the channel pore by virtue of the creation of a reverse turn in the NH_2 terminus that is initiated by a conserved glycine residue at position 12 (Verselis et al., 1994; Purnick P.E., S. Oh, V.K. Verselis, T. Dowd, and T.A. Bargiello, manuscript in preparation). Thus, it is likely that a negative (D2 in Cx26) and a positive (associated with the NH_2-terminal Met residue in both Cx32 and Cx26) charge reside near the cytoplasmic entry of the hemichannels formed by these two connexins. Our previous work also demonstrated that charge substitutions of amino acid residues located at the border of the first transmembrane domain and first extracellular loop may also reverse gating polarity. Consequently, we first examined the role of the amino terminus and first extracellular loop in the voltage dependence of initial currents. The results we present in the following sections show that charged amino acid residues in the amino terminus of Cx26 and Cx32 and in the extracellular loop of Cx26 play a major role.

Role of the Amino Terminus of Cx32

Fig. 6 A illustrates that the initial currents of the heterotypic Cx32/Cx32N2D junctions rectify similarly to those observed in wild-type Cx32/Cx26 heterotypic junctions when expressed in pairs of *Xenopus* oocytes. The effect appears to be due to the electrostatic contribution of the N2D mutation, as the voltage dependence of the initial conductance of Cx32N2E is similar to that of Cx32N2D (Fig. 6 B), and substitutions with neutral amino acids Cx32N2Q and Cx32N2A have little or no effect on the voltage dependence of initial conductance (data not shown). These results suggest that charged amino acid residues in the amino terminus of Cx32 play a substantial role in the rectification of initial currents. However, studies of chimeras in which the first 11 amino acids of Cx26 were substituted for those of Cx32 suggest that residues in other domains may also play a role. For example, the chimera Cx32* Cx26($NT_{1–11}$), which results in the substitution of seven amino acid residues in Cx32, including N2D, did not express junctional currents when paired homo- or heterotypically with Cx26 or Cx32. This result was unexpected as the reciprocal domain substitution, Cx26* Cx32($NT_{1–11}$), forms functional channels [not shown,

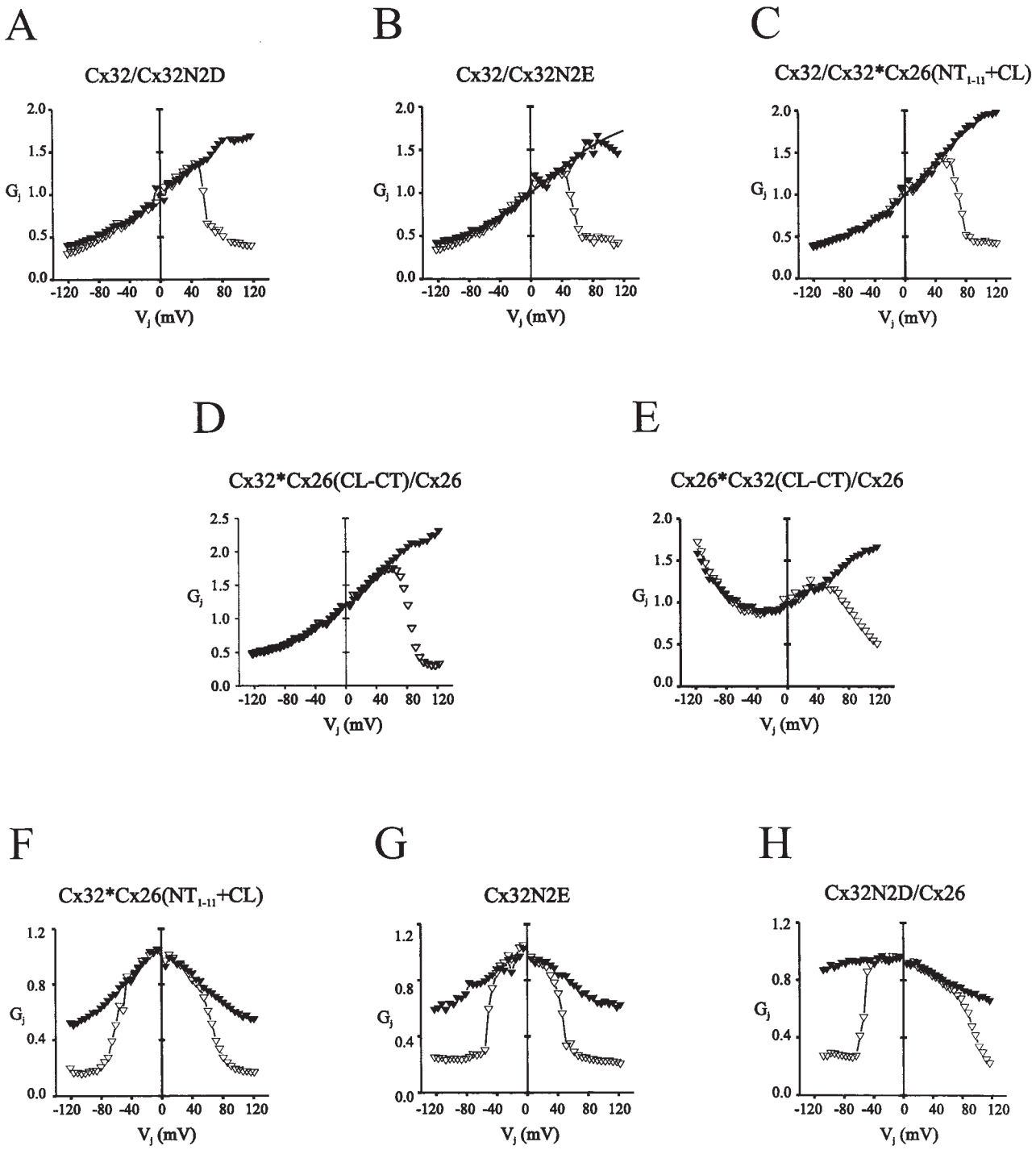

Figure 6. Conductance–voltage relations of mutant and chimeric connexins expressed in pairs of *Xenopus* oocytes. In all cases, junctional conductance is normalized to $V_j = 0$. Initial conductance is depicted by ▼, steady state conductance by ▽. The conductance–voltage relation shown for each junction is representative of at least three separate determinations.

see also Verselis et al., 1994, where Cx26*Cx32($NT_{1–11}$) is designated as Cx26*32NT-V13]. Expression of junctional currents can be restored if the Cx32*Cx26($NT_{1–11}$) chimera also contains the cytoplasmic loop of Cx26; i.e., Cx32*Cx26($NT_{1–11}$+CL). This result suggests that the amino terminus and cytoplasmic loop of Cx26 may interact directly and that this interaction may be required for the expression of junctional currents.

The conductance–voltage relation of the heterotypic Cx32/Cx32*Cx26($NT_{1–11}$+CL) junction is shown in

Fig. 6 C. Notably, the initial conductance of this junction rectifies more steeply (five- vs. threefold over ±120 mV) than does the initial conductance of Cx32/Cx26 junctions (compare Figs. 1 C and 6 C). Other Cx32 chimeric junctions, which contain the cytoplasmic loop of Cx26; Cx32*Cx26(CL–CT)/Cx26 (Fig. 6 D) and Cx32*Cx26CL/Cx26 (not shown) also display increased steepness in initial conductance.

The behavior of the heterotypic junction Cx26*Cx32(CL–CT)/Cx26, in which the CL through CT domain of Cx26 is replaced by that of Cx32, is interesting as the initial conductance increases at larger transjunctional voltages of either polarity of V_j (Fig. 6 E). This change in initial conductance corresponds to a superlinear I–V relation. Also, the gating polarity of the Cx26*Cx32(CL–CT) hemichannel appears to be reversed as steady state conductance only decreases when the Cx26 side of the junction is relatively positive or the Cx26*Cx32(CL–CT) side of the junction is relatively negative. This result is surprising as both Cx26 and Cx26*Cx32(CL–CT) hemichannels have a negatively charged residue at the second position (D2). We suggest that the chimera has a different conformation that effectively reduces the electrostatic contribution of the D2 residue to the voltage sensor of the Cx26*Cx32(CL–CT) hemichannel. We did not observe the expression of junctional currents in homotypic pairings of this hemichannel.

The voltage dependence of initial currents in homotypic junctions formed by Cx32*Cx26($NT_{1–11}$+CL), and Cx32N2E (Fig. 6, F and G) is substantially greater than that observed in Cx32 homotypic junctions. Initial conductance declines by ~50% over ±120 mV_j in both Cx32N2E and Cx32*Cx26($NT_{1–11}$+CL) homotypic junctions. In addition, the shape of the initial conductance–voltage relations of these homotypic junctions differs markedly from that of Cx32 homotypic junctions, declining at small as well as large transjunctional voltages.

The initial conductance of heterotypic junctions Cx32N2D/Cx26, Cx32N2E/Cx26, and Cx32*Cx26($NT_{1–11}$+CL)/Cx26 decreases for either polarity of applied V_j, but substantially more when the Cx26 side of the junction is relatively positive. The conductance–voltage relation of Cx32N2D/Cx26 (Fig. 6 H) exemplifies the behavior of these junctions.

The single channel I–V relations in *Neuro-2a* cells of the fully open Cx32*Cx26($NT_{1–11}$+CL) channel in homo- and heterotypic pairings with Cx32 and Cx26 are shown in Fig. 7. In the case of the homotypic channel, Cx32*Cx26($NT_{1–11}$+CL), the I–V relation of the fully open channel is sigmoidal. Currents decline by ~35–40% at ±120 mV from that predicted by a linear fit of the current trace at ±20 mV (Fig. 7 A). The I–V relation of the fully open Cx32*Cx26($NT_{1–11}$+CL)/Cx26 channel is asymmetric, decreasing more when the Cx26 side of the channel is relatively positive (Fig. 7 B) than when it is relatively negative (compare with Fig. 6 H). Fig. 7 C illustrates that junctional currents rectify when the Cx32/Cx32*Cx26($NT_{1–11}$+CL) heterotypic channel resides in the fully open state; increasing ~4.5-fold (±120 mV) when the Cx32 cell is made relatively negative (note that there are two channels in this record). This rectification is greater than that observed for wild-type Cx32/Cx26 heterotypic junctions (compare Fig. 7 C with 5 F). In all cases, the degree and direction of rectification of Cx32*Cx26($NT_{1–11}$+CL) channels in *Neuro-2a* cells is reasonably well predicted by the macroscopic behavior of initial currents of this junction when they are expressed in pairs of *Xenopus* oocytes. There is similar correspondence between the single channel I–V relation and the macroscopic conductance–voltage relation of the Cx32N2E homotypic junction (data not shown).

Fig. 7 D shows the I–V relation of a Cx32*Cx26($NT_{1–11}$+CL)/Cx26 channel substate that was obtained by applying a −120- to +120-mV ramp to the Cx26 side of the channel. The chord conductance of this substate decreased nonlinearly as the Cx26 side of the junction became more positive. Given the positive gating polarity of both Cx26 and Cx32*26($NT_{1–11}$+CL) hemichannels, this substate most likely resulted from the closure of the Cx32*Cx26($NT_{1–11}$+CL) hemichannel as the channel entered the substate when the Cx32*Cx26($NT_{1–11}$+CL) cell was relatively positive.

In the case of the homotypic Cx32*Cx26($NT_{1–11}$+CL) channel illustrated in Fig. 7 E, single channel currents rectified when the hemichannel in the unstepped cell entered a substate in response to the initial positive polarity of the voltage ramp that was applied to stepped cell (ramped from +120 to −120 mV). This would favor the closure of the V_j gate in the stepped cell as this cell would be relatively positive. As in Fig. 7 D, chord conductance decreased nonlinearly through the substate when the voltage of the stepped cell became more negative.

As noted, the substitution of a single negative charge in the amino terminus of Cx32 is sufficient to make both the initial and steady state conductance–voltage relations of heterotypic mutant/Cx32 junctions resemble that of the Cx32/Cx26 heterotypic junction. However, none of the initial conductance–voltage relations of homotypic Cx32N2D, Cx32N2E, or Cx32*Cx26($NT_{1–11}$+CL) junctions resemble that of homotypic junctions formed by Cx26 (compare Figs. 6, F and G, and 7 A with Figs. 1 B and 4 G). Also, the initial conductance–voltage relation of junctions formed by pairing these mutant hemichannels heterotypically with Cx26 is markedly asymmetric (illustrated by Figs. 6 H and 7 B). These results indicate that the molecular de-

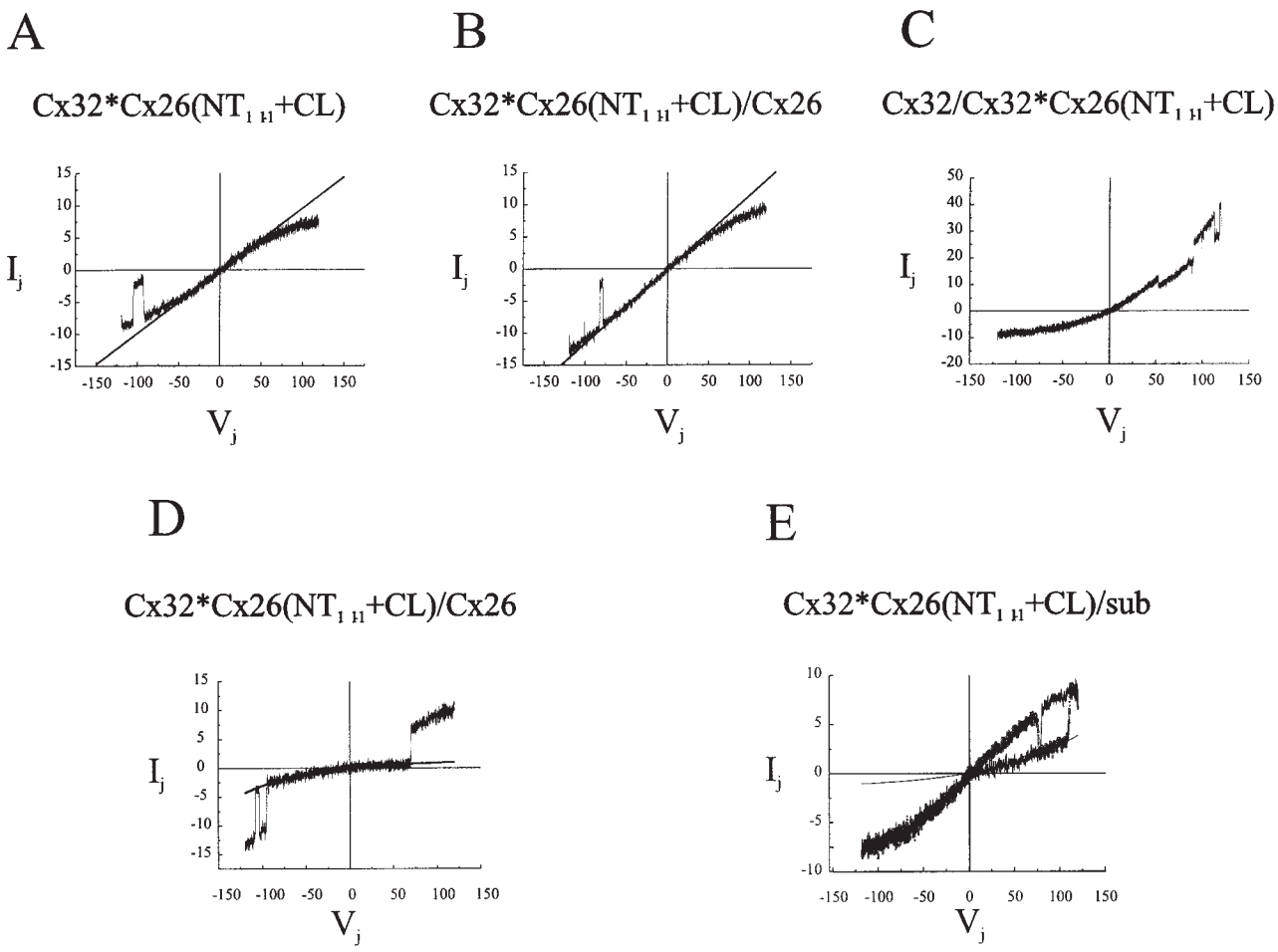

Figure 7. I–V relations of fully open and substates of Cx32*Cx26(NT_{1-11}+CL) in homo- and heterotypic pairing configurations with Cx26 and Cx32 in *Neuro-2a* cells. In all cases, the I–V relations were obtained with 6-s voltage ramps over ±120 mV. The value of V_j shown is the potential of the hemichannel on the right hand side of the pairing designation. In C, there were two intercellular channels. Two current traces from subsequent voltage ramps to the same cell pair were superimposed in E. (E) The "sub" on the right hand side of the pairing designation indicates that this hemichannel had entered into a substate in response to positive V_j. The I–V relations shown are representative of at least 50 voltage ramps that were obtained in each of several different cell pairs.

terminants of initial conductance differ in Cx26 and Cx32 channels.

Role of the Amino Terminus of Cx26

When the Cx26 side of the heterotypic Cx26D2N/Cx26 junction is relatively positive, initial conductance increases as shown in Fig. 8 A. Qualitatively, the voltage dependence of initial conductance is similar, but less steep than is observed in the Cx32/Cx26 junction. This result is consistent with the interpretation that the D2 residue in Cx26 plays a role in the process underlying the open channel rectification of Cx32/Cx26. However, the initial conductance of the Cx32/Cx26D2N junction (Fig. 8 B) does not resemble that observed in Cx32 homotypic junctions as would be expected if the Cx26D2N mutation had converted Cx26 into Cx32. Nor does the initial conductance resemble that of junctions exemplified by Cx32N2D/Cx26 junctions (Fig. 6 H), as would be expected if Cx32 and Cx26 made equal contributions to the rectification of initial conductance. In fact the initial conductance of the Cx32/Cx26D2N junction (Fig. 8 B) rectifies more than that observed in the Cx26D2N/Cx26 junction (Fig. 8 A) and, unlike the Cx32/Cx26 junction, conductance increases when the Cx32 side is relatively negative.

The results obtained with the Cx26D2N mutation must be interpreted cautiously, as the mutation causes a substantial shift in the steady state conductance–voltage relation. A simple implication of this result is that there is a higher probability that the mutant hemichannel resides in a substate at $V_j = 0$. Therefore, it is likely that currents passing through one or more substates make a substantial contribution to the initial currents measured macroscopically in *Xenopus* oocytes when the experimental paradigm described in materials and methods

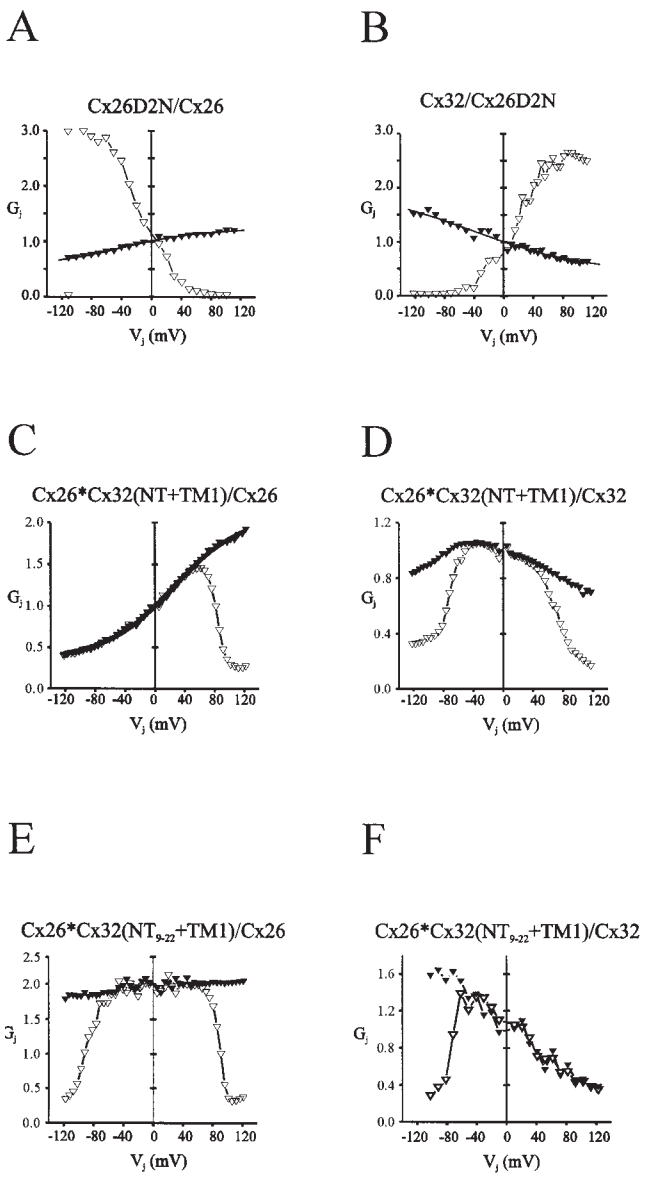

Figure 8. Conductance–voltage relations of mutant and chimeric connexins. In all cases, junctional conductance is normalized to the initial conductance at $V_j = 0$. Initial conductance is depicted by ▼, steady state conductance by ▽. The value of V_j is the potential of the hemichannel on the right-hand side of the pairing designation. The conductance–voltage relation shown for each junction is representative of at least three separate determinations.

is employed. A large shift in the steady state conductance–voltage relation of the Cx26D2N hemichannel towards positivity explains the failure to observe junctional currents in the homotypic Cx26D2N junctions. The conductance–voltage relation inferred for Cx26D2N hemichannels from Cx26D2N/Cx26 junctions predicts that junctional conductance of homotypic Cx26D2N junctions would be substantially reduced at all transjunctional voltages. We have not yet examined the single channel currents of Cx26D2N mutations.

The conductance–voltage relation of Cx26 chimeras containing the NH_2 terminus and first transmembrane domains of Cx32, Cx26*Cx32(NT+TM1), do not display large shifts in their steady state conductance–voltage relations. Consequently, they provide a means of examining the effect of neutralization of the negative charge of the D2 residue on the voltage dependence of initial conductance. Fig. 8 C illustrates that the initial conductance of the heterotypic junction, Cx26*Cx32(NT+TM1)/Cx26, is similar to that of Cx32/Cx26. This result suggests that the Cx26 chimera has adopted Cx32 properties. However, the initial conductance of Cx26*Cx32(NT+TM1)/Cx32 junction is markedly asymmetric (Fig. 8 D), decreasing more when the Cx32 hemichannel is stepped to positive transjunctional voltages. The substitution of either N2D or the first eight amino acids of Cx26 into the amino terminus of the Cx26*32(NT+TM1) chimera results in hemichannels, Cx26*Cx32(N2D+NT+TM1), and Cx26*Cx32($NT_{9–22}$+TM1), whose properties are indistinguishable from those of wild-type Cx26. The conductance–voltage relations of Cx26*Cx32($NT_{9–22}$+TM1)/Cx26 and Cx26*Cx32($NT_{9–22}$+TM1)/Cx32 are shown in Fig. 8, E and F). These results indicate that amino acids downstream of TM1 in addition to the charged aspartate residue (D2) are responsible for the linear initial conductance–voltage relation of Cx26 homotypic junctions.

Role of the First Extracellular Loop

Our previous work indicated that the E1 domain of Cx26 was likely to be involved in the voltage dependence of initial currents, because a chimera in which the first extracellular loop of Cx32 was replaced with the E1 domain of Cx26 to form Cx32*Cx26E1 demonstrated an appreciable asymmetry in the conductance–voltage relation of initial currents when paired with Cx32 (Rubin et al., 1992a; Fig. 9 A). The voltage dependence of initial currents in the Cx32*Cx26E1/Cx32 heterotypic junction (Fig. 9 A) is very similar to that of the Cx26*Cx32(NT+TM1)/Cx32 heterotypic junction (Fig. 8 D). In both cases, initial conductance declines more when the Cx32 hemichannel is stepped to positive potentials. The initial conductance–voltage relations of Cx32*Cx26E1 homotypic and Cx32*Cx26E1/Cx26 junctions do not differ substantially from wild-type Cx32 homotypic and Cx32/Cx26 heterotypic junctions (Fig. 9, B and C) when expressed in pairs of *Xenopus* oocytes. As for the Cx32 wild-type homotypic junction, the I–V relation of the fully open Cx32*Cx26E1 channel does not correspond to the macroscopic data obtained in pairs of *Xenopus* oocytes. When Cx32*Cx26E1 is expressed in *Neuro-2a* cell lines, the I–V relation of the fully open channel is linear (Fig. 9 D).

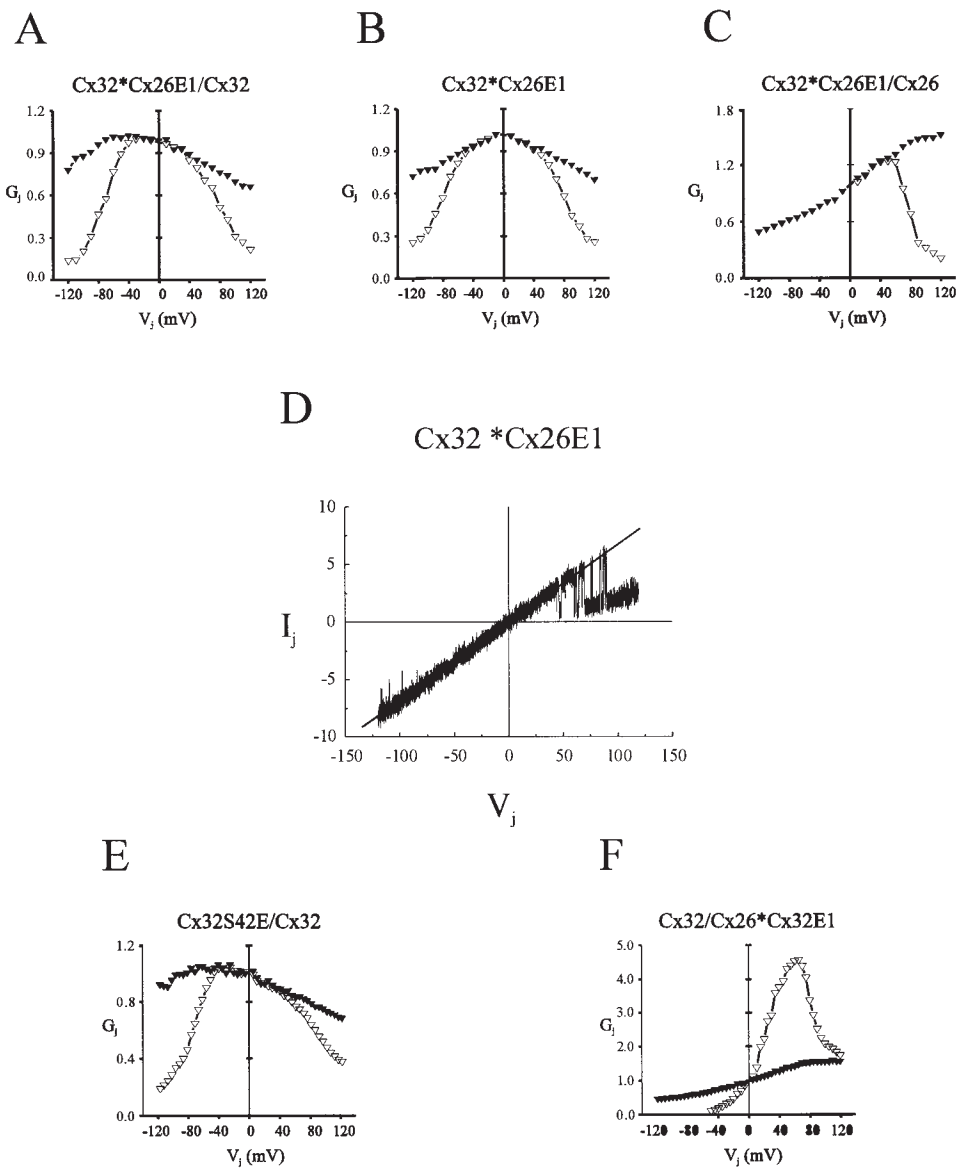

Figure 9. Conductance–voltage relations of mutant and chimeric connexins. In all cases (except D), junctional conductance is normalized to $V_j = 0$. Initial conductance is depicted by ▼, steady state conductance by ▽. The value of V_j is the potential of the hemichannel on the right-hand side of the pairing designation. The conductance–voltage relation shown for each junction is representative of at least three separate determinations. (D) The I–V relation of the open state of the homotypic Cx32* Cx26E1 intercellular channel obtained with 6-s voltage ramp over ±120 mV. The current trace shown is representative of 50 voltage ramps.

The changes in voltage dependence of the Cx26E1 substitution into Cx32 are likely to involve amino acid residues located at the TM1/E1 border as the double mutation, Cx26(K41E,E42S) (previously termed Cx26* ES) displays a steeper initial conductance–voltage relation than does Cx32/Cx26 when it is paired with Cx32 (Rubin et al., 1992a) and some initial conductance reduction at higher transjunctional voltages when this chimera is paired homotypically (Bennett et al., 1993). The effects appear to be localized to residue E42 in Cx26 as the initial conductance–voltage relation of the point mutation, Cx32S42E, in heterotypic pairings with Cx32 (Fig. 9 E) is almost identical to those observed with the chimeras Cx32*Cx26E1 (Fig. 9 A) and Cx26* Cx32(NT+TM1) (Fig. 8 D). Accordingly, the asymmetry in the conductance–voltage relation of the Cx32N2D/Cx26 heterotypic junction (Fig. 6 H) could be explained by the presence of the E42 residue in the Cx26 hemichannel and its absence in the Cx32N2D hemichannel. Thus, the presence of negative charge at residue 42 appears to be an important determinant of the voltage dependence of initial conductance.

The reciprocal chimera, Cx26*Cx32E1, displays a large shift in the steady state conductance–voltage relation in heterotypic pairings with Cx32, as illustrated in Fig. 9 F. Although initial conductance increases in this heterotypic junction with positivity on the Cx26*Cx32E1 side, the large shift in the steady state conductance–voltage relation makes it likely that substates of the Cx26*Cx32E1 hemichannel make a substantial contribution to the initial conductance determined macroscopically and this possibility complicates any quantitative interpretation. We did not observe the expression of junctional currents in Cx26*Cx32E1 homotypic pair-

ings, an observation that may be explained by a negative shift in the $V_{1/2}$ of both hemichannels conductance–voltage relations.

Substitution of Other Domains Does Not Alter the Voltage Dependence of Initial Currents

Reciprocal substitutions of the second extracellular loop of Cx26 and Cx32 have no effect on the voltage dependence of steady state or initial conductance in homo- and heterotypic pairings (Rubin et al., 1992a,b). The initial conductance of homotypic junctions of Cx32 chimeras, which contain one or more of the four transmembrane domains of Cx26 (Cx32*Cx26TM1, Cx32*Cx26TM2, Cx32*Cx26TM3, and Cx32*Cx26TM4) are similar to homotypic junctions formed by Cx32, and the heterotypic junction Cx32/Cx26*Cx32(TM4-CT) behaves like wild-type Cx32/Cx26 (data not shown). Also, a truncation of the Cx32 carboxyl terminus after TM4 (at residue 248) has little effect on the voltage dependence of initial conductance in homo- and heterotypic pairings with Cx32 and Cx26 (data not shown). Although the substitution of the TM1 domain does not cause marked changes in the transjunctional voltage dependence of initial conductance, it does alter the steady state conductance–voltage relation (data not shown). This result suggests that some conformational changes have occurred.

These data indicate that substitutions involving the second extracellular loop, the four transmembrane domains and the carboxyl terminus have little or no effect on the voltage dependence of initial conductance observed in junctions formed by Cx26 and Cx32. However, as described above, changing amino acids positioned in the amino terminus and first extracellular loop appear to have pronounced effects. Although the cytoplasmic loop alters the voltage dependence of initial conductance, it is not clear if this is the result of a direct electrostatic effect or an indirect effect caused by changes in the conformation of the amino terminus.

discussion

Molecular Determinants of Electrical Rectification

Based on the single channel data presented in this paper, it is apparent that the voltage dependence of initial conductance observed in the heterotypic Cx32/Cx26 channel arises as a consequence of the rectification of ionic currents through open channels rather than by conformational changes associated with voltage-dependent gating. It is remarkable that the I–V relations of both Cx32 and Cx26 homotypic channels expressed in *Neuro-2a* cell lines are essentially linear. Evidently, the union of Cx32 and Cx26 hemichannels results in an asymmetry in the structure of the heterotypic channel that produces the rectifying current–voltage relation. The union of like hemichannels to form a complete intercellular channel always results in symmetric, although not necessarily linear, I–V relations. For example, the I–V relation of homotypic Cx32*Cx26($NT_{1–11}$+CL) channels is sigmoidal (Fig. 7, A and E). Asymmetric conductance–voltage relations may also result if the channels display dependence on the absolute voltage difference between the inside and outside of the cells (termed V_{i-o} or V_m). However, this form of voltage dependence does not underlie the open channel I–V relations described in this study.

Our previous results have indicated that charged amino acid residues, positive (M1) and negative (D2) in Cx26 and positive only (M1) in Cx32, are responsible for the difference in the V_j -dependent gating polarity of Cx26 and Cx32 hemichannels. We proposed that these residues are located near the cytoplasmic entrance of the channel pore based on their ability to sense transjunctional voltage and the accepted membrane topology of gap junctions. These charges may account for the slight anion selectivity of homotypic Cx32 channels (Oh et al., 1997) and the slight cation selectivity of Cx26 homotypic channels (Veenstra, 1996). The data presented in this paper indicate that these same charged amino acid residues are also involved in the mechanism underlying the voltage dependence of initial conductance.

The observations that the substitutions of the neutral second amino acid residue of Cx32 with negatively charged amino acid residues alter the initial conductance–voltage relation and that neutral amino acid substitutions do not change initial conductance are consistent with an electrostatic effect. The increased steepness of the rectification observed in the Cx32/Cx32*Cx26($NT_{1–11}$+CL) junction (Figs. 6 C and 7 C) may arise from an interaction between the CL and NT domains that alters the position of the negatively charged residue located in the amino terminus of this chimera. Alternatively, it may reflect an electrostatic effect of charged residues that differ in the CL domain in Cx32 and Cx26. Of the 38 amino acids present in the cytoplasmic loop of Cx26, 50% are charged, 12 positive and 7 negative. Of the 37 amino acid residues in the CL domain of Cx32, 6 are positively and 5 are negatively charged. Nine charges (five positive and four negative) are conserved between the two connexins. Consequently, it is difficult to assess whether the effect of the cytoplasmic loop on open channel rectification is a direct effect of specific charged amino acid residues, or if this domain exerts its effect indirectly by changing the conformation of the NH_2 terminus.

It is apparent that the substitution of a negative charge into NH_2 terminus of Cx32 does not recreate the properties of Cx26 homotypic junctions, since the

I–V relations of Cx32*Cx26(NT_{1-11}+CL) and Cx32N2E homotypic channels are sigmoidal (e.g., Fig. 7 A). Therefore, other charged residues must also influence ionic flux in Cx26 channels. The asymmetry in the voltage dependence of initial currents observed in the Cx32*Cx26E1/Cx32 junction (Fig. 9 A) indicates that the E1 domain of Cx26 is also involved. The negatively charged E42 residue in Cx26 is the best candidate, as the initial conductance–voltage relation of the point mutation Cx32S42E paired heterotypically with Cx32 is almost identical to that of Cx32*Cx26E1/Cx32 (Fig. 9 E). The view that E42 plays a role in the expression of the voltage dependence of initial conductance is further supported by the increased steepness of the voltage dependence of initial conductance observed in the Cx32/Cx26(K41E,E42S) junction (Rubin et al., 1992a). We have not ruled out the possibility that other charged amino acid residues in E1 play a role. The initial conductances of chimeric channels containing the second extracellular loop (E2), the four transmembrane domains (TM1, TM2, TM3, and TM4), and the carboxyl terminus differ little from wild type. If any charged residues in these domains are involved in the voltage dependence of initial conductance, they are likely to be conserved in Cx26 and Cx32.

Electrodiffusive Model of the Observed Electrical Rectification

The results presented in this paper indicate that charged amino acid residues located in the amino terminus and first extracellular loop play a major role in shaping the I–V relations of channels formed by Cx26 and Cx32. In the following sections, we examine whether these charges can account for the I–V relations of wild-type and mutant channels presented in this paper by using the electrodiffusive model of Chen and Eisenberg (1993) that numerically solves the PNP equations in one dimension.

The PNP model of Chen and Eisenberg (1993) is attractive in that it promises to predict the fluxes and current passing through a channel in all experimental conditions once the distribution of permanent (fixed) charge on an ion channel is known (Chen et al., 1997). The theory has been used successfully to describe permeation through a large diameter ($\sim$8 Å) synthetic ion channel (LS channel) using only four adjustable parameters; the diffusion coefficients of two ions in the channel pore and the distribution and density of fixed charge at the ends and central region of the channel (Chen et al., 1997). The availability of a large data set, obtained using 15 different ionic solutions, allowed reliable estimates of these parameters and may have provided a unique solution to the question of charge distribution and ionic mobility in the synthetic channel. However, the approach may provide limited structural information on the LS channel since Chen et al. (1997) state that it is likely that more than one atomic structure would give the same average parameters.

In this study, we adopt a different strategy since we have very limited ionic data for any given channel (at best two ionic conditions for Cx32 channels), but we have information describing how the I–V relations are changed by substitutions of charged amino acid residues in different regions of Cx32 and Cx26 in several different pairing combinations. We seek to determine whether we can use our molecular studies to derive a set of charge distributions that when incorporated into the PNP model will lead to I–V relations comparable with those observed in homotypic and heterotypic pairings of wild-type and mutant hemichannels. In our use of PNP theory, we vary only the magnitude, the position, and the width of fixed charges that we infer from our molecular studies. We use a fixed pore geometry of 7 Å in radius and 120 Å in length. The cation and anion mobilities are set to values of the aqueous bulk solution mobilities of Cs and Cl (2.06 and 2.03 $\cdot$ 10^{-5} cm^2 s^{-1}), the solutions used in single channel experiments that were performed. The ion concentrations were 150 mM in the symmetric salt case, and 15 and 150 mM in the case of 1:10 salt gradients. The dielectric constant for the channel pore and the membrane were fixed at 80 and 4, respectively (the default values of the PNP computer program). The I–V relations obtained were not very sensitive to changes in the value of the dielectric constant assigned to the channel pore in the 150-mM salt case using fixed charges $> \pm 1$ *e*. The PNP model appears to be quite sensitive to reductions in the dielectric constant of the pore when ionic concentrations and the values assigned to fixed charges are both reduced (for example, to 15 mM and 0.1 *e*, respectively, for the charge distribution shown in Fig. 10 C). This observation most likely reflects the "charge screening" property of the PNP model. The input file for the pore surface charge was generated using the PNP Windows computer program of Stephen Traynelis' group (Emory University, Atlanta, GA) using the program's defaults (sigmoid, smooth charge points = 7). In the case where more than two charges are modeled, the charge input file was assembled in overlapping pairwise combinations using Microcal Origin software and saved as PAS or TXT files in Programmers Notepad. Output files (I–V relations, anion and cation fluxes, and chord conductances) were generated using the PNP computer program of Dr. Duan P. Chen (Rush Medical College, Chicago, IL) using the unmodified Poisson Equation. The Fortran version of the computer program was compiled in C^{++} by Brady Trexler (Albert Einstein College of Medicine).

We restrict our use of the PNP model to channels for which we have single channel records. We did not at-

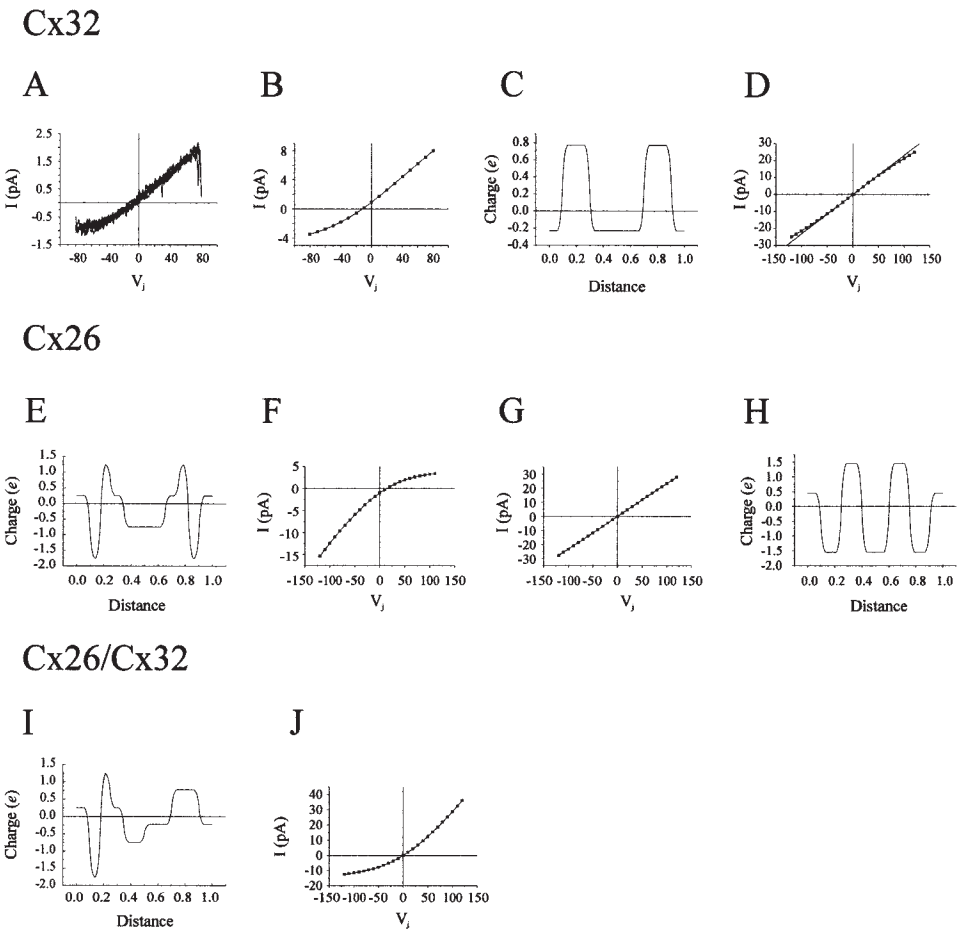

Figure 10. Charge distribution models and I–V relations of Cx32 and Cx26 channels derived from the PNP model. (A) Observed reversal potential of a Cx32 homotypic channels in a 1:10 salt gradient (15 mM CsCl: 150 mM CsCl, see Oh et al., 1997, for details of the method employed). Six consecutive traces from one experiment are shown, E_{rev} is −10.5 mV. The V_j plotted is the voltage applied to the cell containing the low-salt concentration. The membrane potential of the cell containing the high salt solution was 0 mV. (B) The I–V relation for a Cx32 homotypic channel obtained with the PNP model using the charge distribution model shown in panel C and a 1:10 salt gradient (15 mM CsCl:150 mM CsCl). The predicted E_{rev} is −11 mV with the conditions specified in A. (■) Current values calculated by the PNP model at the voltages shown. (C) Intra-pore surface charge distribution modeled for a Cx32 homotypic channel. The charge distribution is presented as a smooth curve although the input file to the computer program specifies 100 points distributed equally over the electrical distance. (D) The I–V relation of Cx32 homotypic channels obtained with the PNP model using the charge distribution profile shown in C and 150 mM symmetric salt condition. The straight line is a linear fit of the current trace to points lying between ±40 mV. (E) Intrapore surface charge distribution model for Cx26 homotypic channels. (F) The I–V relation of Cx26 homotypic channels using the charge profile shown in E and asymmetric ion conditions specified in A. The predicted reversal potential is ∼10 mV. (G) The I–V relation of Cx26 homotypic channel obtained with the PNP model using the charge profile shown in E. (H) An alternative Cx26 surface charge distribution model that results in a linear I–V relation (see text for details). (I) Intrapore surface charge distribution model for Cx26/Cx32 heterotypic channels using the charge distributions shown in C and E (see text for details). (J) The I–V relation of the Cx26/Cx32 channel obtained with the PNP model using the charge distribution shown in I. The V_j plotted is the voltage applied to the Cx26 side of the channel (0.0–0.5 electrical distance).

tempt to use any fitting algorithms, as we feel that this approach is premature in the absence of a larger data set that includes a variety of ionic conditions. The availability of additional ionic data would be helpful in distinguishing among alternative charge distribution models, but such data are lacking at present, and additional ionic data are not easily obtained for intercellular channels expressed in cells.

Models of Wild-Type Channels

Initially, we explored a PNP model of Cx32 with a charge step of +6 *e* located at either end of the open channel, with the rationale that each of the six connexin subunits that form a hemichannel would contribute one positive charge. The I–V relation of a channel with this charge distribution that resulted with the PNP model was quite similar to the I–V relation observed for Cx32 homotypic channels in symmetric 150-mM CsCl solutions (deviating from linearity by ∼5% at ±120 mV, not illustrated). However, although not unexpectedly, the PNP-modeled channel was almost ideally anion selective in 15 mM:150 mM CsCl solutions. Virtually all the current was carried by the anion over the entire voltage range explored in the model (±120 mV) and the predicted reversal potential was approximately −58 mV in the 1:10 salt gradient of this ionic strength. A reversal potential approximating that obtained for Cx32 homotypic channels (approximately −10 mV; see Fig. 10 A) could be obtained by incorporating a baseline charge of −1.5 *e*. The baseline charge in the computer model could be interpreted as a smearing of a negative

charge along the length of the pore surface, perhaps reflecting the negative charge contribution of backbone carbonyls or the negative charge of side chains of pore-lining amino acids. Amino acids such as serine, which are believed to carry partial negative charges (see note 4 in Chen et al., 1997), may also be involved. The PNP model employed does not consider the effects of fixed charges on the distribution of ions outside the pore. Consequently, we could not consider the extent to which fixed charges near the channel entry would alter the local ionic environment outside the channel pore and influence the ionic selectivity of the channel by this mechanism. The incorporation of a baseline charge resulted in a significant deviation from linearity in the I–V relation of the modeled channel with all symmetric salt conditions explored (10–500 mM). Consequently, we explored the I–V relations of channels in which the magnitude of the charge step was reduced. Using a charge step of $+1$ *e*, we were able to find several intra-pore charge distributions that when used as inputs to the PNP model resulted in I–V relations that closely resembled the I–V relation observed for Cx32 homotypic channels in the 1:10 salt gradient employed (see Fig. 10, A–C). The charge distribution shown in Fig. 10 C gives the I–V relation shown in Fig. 10 D in symmetric salt case. The PNP model is expected to change the shape of the I–V relation as a function of ion concentrations (charge screening). Consistent with this expectation, the I–V relation shown in Fig. 10 D (150 mM) becomes more sigmoidal at an ion concentration of 10 mM (not illustrated) and substantially less but still noticeably sigmoidal at ion concentrations of 500 mM (not illustrated). It is tempting to speculate that reduced charge screening due to a markedly lower concentration of permeant anions may contribute to the greater nonlinearity of Cx32 channels when they are examined in CsCl-dialyzed cells compared with undialyzed *Xenopus* oocytes.

Although the shapes of the I–V relations observed correspond closely to those obtained with the PNP model with the charge distribution and parameters used, the predicted single channel conductance is substantially greater than observed (227 vs. 70 pS at ± 60 mV). This problem may be solved by reducing the diffusion coefficients of the ions in the pore, as done by Chen et al. (1997) in the synthetic channel. If the mobility of both the cation and anion are reduced to $0.7 \cdot 10^{-5}$ $cm^2\,s^{-1}$ from the initial values of 2.06 and $2.03 \cdot 10^{-5}$ $cm^2\,s^{-1}$, the single channel conductance closely approximates that observed (70 pS at ± 60 mV). The reductions in ionic mobilities we employ are much less than those used by Chen et al. (1997) in the PNP model of the synthetic LS channel. In that study, the mobility of K^+ was reduced 10-fold while that of Cl^-, 100-fold. The difference perhaps reflects the substantially smaller radius of the LS channel (4 vs. 7 Å). The reduction in ionic mobilities does not alter the shape of the I–V relation of Cx32 (not illustrated). The contribution of friction in the channel pore to ion permeation has been discussed recently by Laio and Torre (1999).

The results of the molecular analysis indicate that the I–V relation of Cx26 channels is likely to be determined by external positive and negative charges and an internal negative charge. Following these considerations, we modeled the charge distribution of Cx26 as illustrated in Fig. 10 E. The charge associated with the D2 residue was set to -2 *e*, the positive charge in the amino terminus set to $+1$ *e*, and the internal charge (E42) was set to -1 *e* as this residue may be located at some distance from the channel lining. We justify the increased magnitude of the D2 charge by considering that negative charge substitutions into the amino terminus of Cx32 appear to dominate the effect of the fixed positive charge in polarity reversal of V_j dependence. We also incorporated a baseline charge of $+0.25$ *e* to make the Cx26 channel slightly cation selective in 150 mM:15 mM CsCl gradients (Fig. 10 F) in consideration of the results reported by Veenstra (1996). The sign of the baseline charge used here is opposite that for Cx32, and we cannot invoke a comparable physical interpretation consistent with that invoked for Cx32. It is possible that the difference in ion selectivity of Cx32 and Cx26 channels is influenced by other charged residues located within the channel and that the incorporation of the baseline charge mimics their effect in both Cx26 and Cx32. Alternatively, the difference in selectivity may be due to the effects of surface charges that change the local ionic environment near the channel entry. As the PNP model employed does not consider the effects of fixed charge outside the ion pore, we could only approximate the weak cation selectivity of the Cx26 channel by incorporating a small positive baseline charge. The I–V relation resulting from the application of the PNP model with this charge distribution model is linear (Fig. 10 G), like that observed for Cx26 homotypic channels, but the single-channel conductance is somewhat larger than observed (220 compared with 150 pS). The incorporation of the baseline charge does not alter the linearity of the I–-V relation of the Cx26 homotypic channel.

An alternative charge distribution model (Fig. 10 H) also results in a linear I–V relation and a slightly cation selective channel (not shown), but in this case the predicted single channel conductance is identical to that observed (150 pS, not shown).

We modeled the charge distribution of the heterotypic Cx26/Cx32 channel (Fig. 10 I) by merging the charge distribution of half the Cx26 channel shown in Fig. 10 E (i.e., covering the electrical distance from 0.0 to 0.5) with that of Cx32, shown in Fig. 10 C (covering

the electrical distance from 0.5 to 1.0). The charge distribution at the point of contact was recalculated by using the Windows PNP program of Traynelis to remove the sharp discontinuity that would otherwise result. The I–V relation resulting from the PNP model (Fig. 10 J) is almost identical to that observed for single Cx26/Cx32 channels, with current increasing approximately threefold when the Cx26 side of the channel is made relatively positive (−12.4 pA at −120 mV to 36.2 pA at 120 mV). The single channel conductance of the modeled channel can be made identical to that observed by reducing ion mobilities to $0.85 \cdot 10^{-5}\,cm^2\,s^{-1}$.

The charge distribution model formed by combining the right half of the charge distribution shown in Fig. 10 C with the left side of the charge distribution shown in Fig. 10 H also resulted in an I–V relation that resembled that of Cx32/Cx26 heterotypic channels, rectifying 2.7-fold at ±120 mV (increasing when the Cx26 side of the channel is positive).

*Models of Cx32*Cx26($NT_{1–11}$+CL) Channels*

In the model of the Cx32*Cx26($NT_{1–11}$+CL) channel, the charge profile of Cx26 shown in Fig. 11 A was modified by removing the central charge (−1 *e*) associated with E42 in Cx26 and moving the external charges outward (the charge step was initiated at an electrical distance of 0.025 rather than 0.1), but the magnitude of the external charges was not altered. The change in position of these charges was required to produce a charge distribution model that could replicate the experimentally observed I–V relations in all pairing combinations involving the Cx32*Cx26($NT_{1–11}$+CL) hemichannel. The baseline charge was increased by 0.25 *e* to 0.5 *e* to maintain the expected moderate cation selectivity of this channel (E_{rev} = −10 mV in 1:10 salt gradient, not shown). The charge profiles for Cx26/Cx32*Cx26($NT_{1–11}$+CL) and Cx32*Cx26($NT_{1–11}$+CL)/Cx32 are shown in Fig. 11, B and C, respectively. The I–V relations given by the PNP model for the homotypic Cx32*Cx26($NT_{1–11}$+CL) channel, and heterotypic Cx26/Cx32*Cx26($NT_{1–11}$+CL) and Cx32*Cx26($NT_{1–11}$+CL)/Cx32 channels closely resemble the observed I–V relations (compare Fig. 11, D–F with Fig. 7, A–C). The small difference in the modeled and observed single channel conductances could be further reduced by decreasing the mobilities of ions in the PNP model ($1.4 \cdot 10^{-5}\,cm^2\,s^{-1}$ for the homotypic channel, $1.2 \cdot 10^{-5}\,cm^2\,s^{-1}$ for the heterotypic Cx26 channel, and $0.9 \cdot 10^{-5}\,cm^2\,s^{-1}$ for the heterotypic Cx32 channel).

The I–V relations of homotypic junctions formed by Cx32N2E and Cx32N2D and their heterotypic junctions with Cx32 and Cx26 can be explained using charge distribution models similar to those employed to explain the behavior of the Cx32*Cx26($NT_{1–11}$+CL) channels (not shown). However, using half of the charge distribution model shown in Fig. 10 H for Cx26 to form a model of Cx26/Cx32*Cx26($NT_{1–11}$+CL) channel produced a nearly symmetric sigmoidal I–V relation (not shown) that did not correspond to the I–V relation observed experimentally. As we were not able to find an alternate charge distribution model for Cx32*Cx26($NT_{1–11}$+CL) that would provide the observed I–V relation, we believe that the Cx26 charge distribution model shown in Fig. 10 H is unlikely to be correct.

*Models of Cx32*Cx26E1*

As detailed above, there is good qualitative agreement between the I–V relations obtained with the PNP model using the charge distributions inferred from the molecular studies and those observed in this study. However, the linearity of the I–V relation of the Cx32*Cx26E1 homotypic channel cannot be explained by charge distribution models using only the identified charges analyzed so far. We were surprised to be unable to obtain a linear I–V relation for Cx32*Cx26E1 using the PNP model with the identified external and internal charges (M1 and E42). The I–V relation of a channel containing only the central charges (E42) is linear (not shown), while the I–V relation of a channel containing an external charge at either end can be linearized by moving the charges centrally (not shown) in the PNP analysis. Yet all models that considered both charges together were characterized by substantially sigmoidal I–V relations (not shown). A nearly linear I–V relation could be obtained by the PNP model if one incorporated a partial negative charge near the ends of the charge distribution model for Cx32*Cx26E1. The conserved tryptophan residue at the third amino acid position (W3) is a reasonable candidate for the formation of this negative charge if one proposes that the tryptophan residue adopts a conformation such that the negative component of the electrostatic surface potential of the aromatic ring of the tryptophan residue is oriented parallel to the channel pore. We did not consider the positive component of the electrostatic surface potential. The aromatic ring of the tryptophan residue has a permanent quadrupole moment and it is believed that its electrostatic effect is important in cation–π interactions (Mecozzi et al., 1996). Favorable electrostatics between an ion and the indole ring of tryptophan have been reported to facilitate the cation conductance of gramicidin A channels (Becker et al., 1991; see also Dorigo et al., 1999). Kumpf and Dougherty (1993) have proposed that cation–π interactions at conserved aromatic amino acids may be responsible for the ion selectivity of potassium channels.

The charge distribution used and the resulting I–V relation of this class of model after the application of

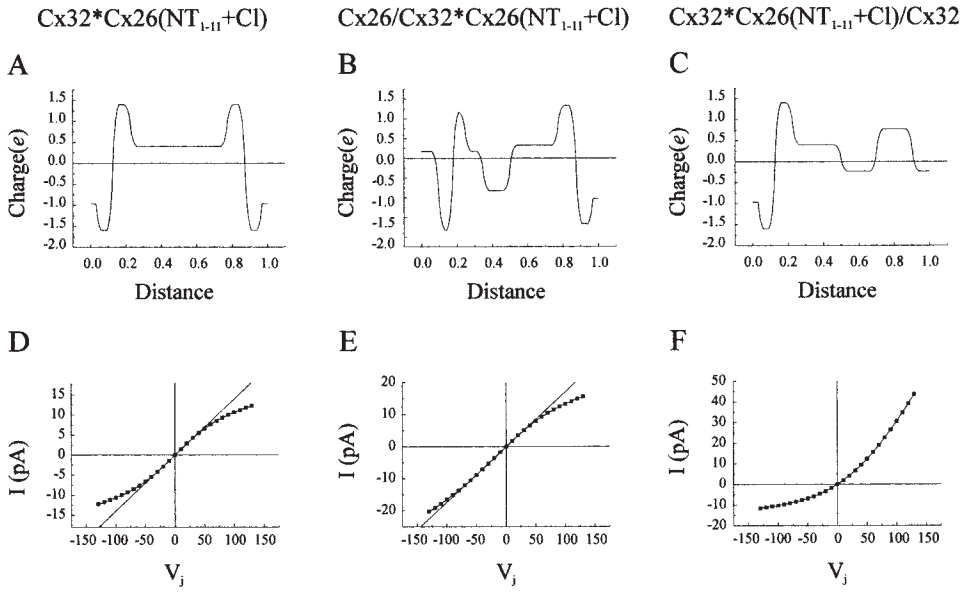

Figure 11. Charge distribution models and I–V relations of Cx32*Cx26(NT_{1-11}+CL) channels derived from the PNP model. (A–F) The I–V relations of channels obtained with the PNP model using the charge distributions shown in A–C are presented in D–F. The V_j plotted is the voltage applied to the hemichannel that would correspond to the electrical distance from 0.0 to 0.5 in A–C. The straight lines in D and E are linear fits to the data points lying between +40 and −40 mV.

the PNP model are illustrated in Fig. 12, A and D. However, the incorporation of a negative charge at the W3 position alters the predicted I–V relation of Cx32 homotypic channels and Cx26/Cx32 heterotypic channels. The I–V relation of Cx32 becomes linear and notably the predicted reversal potential in a 1:10 salt gradient is close to that observed without the incorporation of a baseline charge (not shown). Also, the predicted I–V relation of Cx26/Cx32 rectifies much less, approximately twofold over ±120 mV (not shown). Interestingly, a channel with the charge distribution shown in Fig. 12 B has a predicted I–V relation that closely resembles wild-type homotypic Cx32 channels (Fig. 12 E). In this case, the magnitude of the charge at W3 was reduced to −0.25 *e*, and a central charge of −0.5 *e* was introduced. It is possible that this charge corresponds to residue E41 in Cx32 and that the charge profile shown in Fig. 12 B more closely approximates that of Cx32 than the one shown in Fig. 10 C. Consequently, we explored the effect of incorporating the negative charges associated with residues W3 and E41 in a model of the heterotypic Cx26/Cx32 channel. The modeled charge distribution is shown in Fig. 12 C. The resulting I–V relation closely resembles that of Cx26/Cx32, rectifying 2.8-fold (−14.3 pA at −120 mV/40.7 pA at +120 mV). The single channel conductance

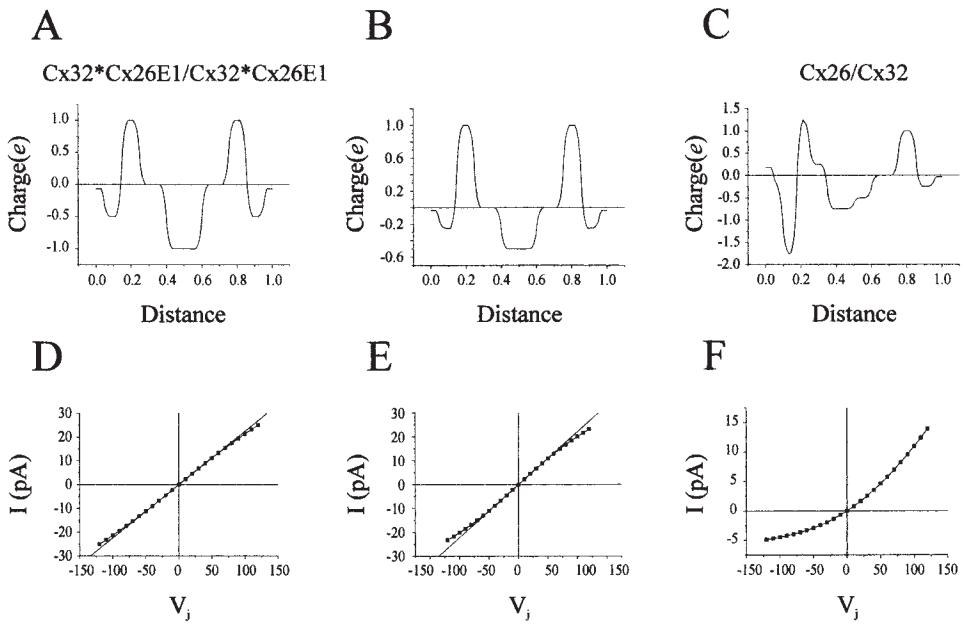

Figure 12. Charge distribution models and I–V relations of channels presumed to contain a centrally located negatively charged residue. (A–F) The I–V relations of channels obtained with the PNP model using the charge distributions shown in A–C are presented in D–F. The V_j plotted is the voltage applied to the hemichannel that would correspond to the electrical distance from 0.0 to 0.5. The straight lines in D and E are linear fits to the data points lying between +40 and −40 mV.

of the modeled channel is three times greater than that actually observed, but can be adjusted by reducing the intrapore ionic mobilities of both the anion and cation to $0.7 \cdot 10^{-5}\,cm^2\,s^{-1}$ from the bulk solution mobilities of Cs and Cl. The I–V relation of the resulting channel is shown in Fig. 12 F. The incorporation of a negative charge ($-0.5\,e$) associated with E41 into the charge distribution models of Cx32*Cx26(NT_{1-11}+CL) channels (Fig. 11) does not substantially alter the resulting I–V relations obtained with the PNP model. The effect of this charge on the I–V relation obtained for the Cx26/Cx32*Cx26(NT_{1-11}+CL) channel is illustrated in Fig. 13.

Extension of the Model to Other Channels

We did not attempt to apply PNP theory to model the behavior of the remaining junctions for which we have no single-channel data. We expect that the I–V relations that can be inferred from the macroscopic conductance–voltage relations could be predicted by the charge distribution models we present for Cx32, Cx26, Cx32*Cx26(NT_{1-11}+CL) and Cx32*Cx26E1 with only minor modifications. The only notable exception is the superlinear I–V relation that would correspond to the macroscopic conductance–voltage relation of the Cx26*Cx32(CL–CT)/Cx26 heterotypic junction (Fig. 6 E). The apparent reversal of the V_j gating polarity of the Cx26*Cx32(CL–CT) hemichannel suggests that a conformational change has taken place that effectively removes the D2 residue from the transjunctional field. In barrier models, superlinear I–V relations are easily explained by the presence of a dominant central barrier. We did not find a reasonable way to obtain a superlinear I–V relation with the PNP model, although superlinear I–V relations have been obtained with the PNP2 model (Nonner and Eisenberg, 1998). Superlinearity can be obtained with the PNP model we use by placing a widely dispersed charge in the center of the channel and reducing the mobility of the oppositely charged ion by several orders of magnitude to $10^{-9}\,cm^2\,s^{-1}$. Further analyses of this interesting junction await confirming single-channel data.

Summary of the Application of the PNP Model

The preceding sections illustrate how the results of the molecular analyses could be used in conjunction with the PNP model of Chen et al. (1997) to derive a consistent set of charge-distribution models for hemichannels formed by Cx32, Cx26, and NH_2-terminal charge substitutions of Cx32. For the most part, the inferred charge distribution models reasonably reproduced the observed single-channel I–V relations of homotypic and heterotypic channels formed by these connexins when used as input parameters of the PNP model. The only notable exception was the I–V relation of the homotypic Cx32*Cx26E1 channel. The charge distribution that was inferred for this channel, containing an internal negative charge contributed by the E42 resi-

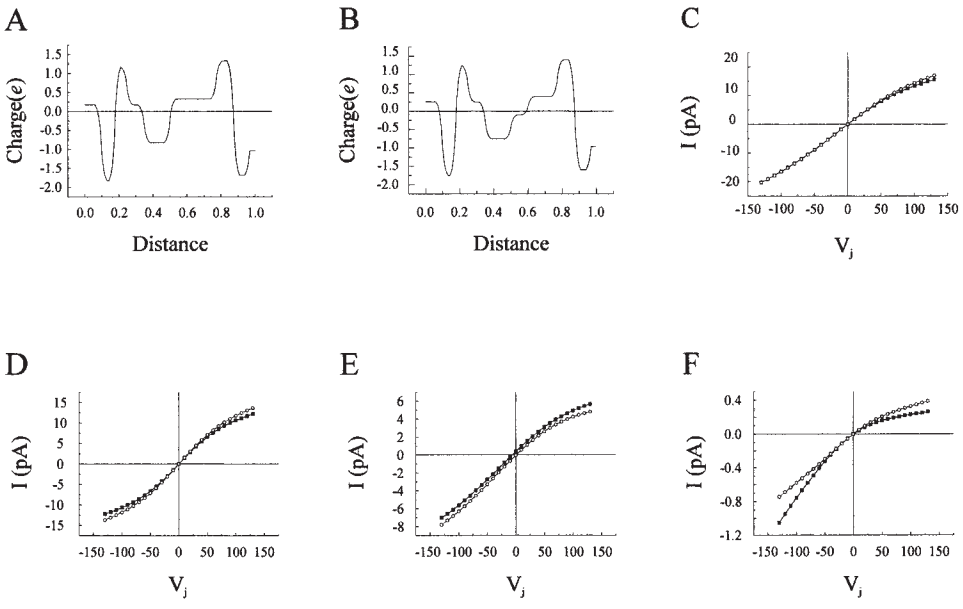

Figure 13. Sensitivity of the PNP model to changes in intrapore surface charge. (A) A surface charge distribution model of the pore of the Cx26/Cx32*Cx26(NT_{1-11}+CL) channel (as shown in Fig. 11). (B) An alternate charge distribution model of the pore of the Cx26/Cx32*Cx26(NT_{1-11}+CL) channel that incorporates a negative internal charge that may correspond to residue E41 in Cx32 (see Fig. 12 and text). (C) The I–V relations that result from the application of the PNP model using the charge distribution models shown in A (■) and B (○) in symmetric 150-mM salt solutions. (D) The I–V relations of homotypic Cx32*Cx26(NT_{1-11}+CL) channels in symmetric 150-mM salt solutions. (■) I–V relation of a homotypic channel that is based on the charge distribution corresponding to the right half (electrical distance 0.5–1.0) of A (see also Fig. 11). (○) I–V relation of a homotypic channel that is based on the right half of the charge distribution model shown in B. (E) The I–V relations of the charge distribution models shown in A (■) and B (○) when the ionic concentrations used in the PNP model were asymmetric (15 mM:150 mM). (F) The I–V relations resulting from the charge distribution models shown in A (■) and B (○) when the ionic concentration specified in the PNP model was reduced to 15 mM.

due of Cx26 in addition to the external positive charge associated with residue (M1), did not reproduce the observed linear I–V relation when it was used as an input to the PNP model. Exploration of other charge distributions with the PNP model indicated a potential solution; the involvement of a partial negative charge (possibly reflecting the negative component of electrostatic surface potential of the indole ring of the W3 residue). Explorations of other charge distributions with the PNP model also suggested that the negative charge of the Cx32E41 residue may play a role in determining the I–V relations of the channels examined. Additional molecular studies are required to confirm the hypothesized role of these charged residues in shaping the I–V relations of Cx32 and Cx26 channels.

It is important to stress that the set of charge distribution models provided above are probably not unique, in that there are likely to be other sets of charge distribution models that may also consistently describe the available set of experimentally observed I–V relations. This statement is not meant to imply that all charge distribution models that were examined in the current study could satisfactorily account for the entire experimental data set. For example, the class of charge distribution model for Cx26 illustrated in Fig. 10 H did not give rise to the experimentally observed I–V relation for the Cx26/Cx32*Cx26($NT_{1–11}$+CL) channel, although it worked reasonably well in reproducing the I–V relations of Cx26 homotypic and Cx32/Cx26 heterotypic junctions. We were unable to find an alternate charge distribution of Cx32*Cx26($NT_{1–11}$+CL) that could remedy this discrepancy and continue to adequately describe the behavior of other channels. Similarly, the model appeared to be quite sensitive to changes in the position of charges located near the entry of the Cx32*Cx26 ($NT_{1–11}$+CL) hemichannel. As described above, the charges in this region had to be moved outward relative to those used in the charge distribution model of Cx26 to satisfactorily reproduce the I–V relations of homotypic and heterotypic channels observed for this chimera. The PNP model appears to be sensitive to changes in the position of charges in the class of charge distribution model exemplified by the Cx32* Cx26($NT_{1–11}$+CL) chimera, but, as described below, less sensitive to other changes in charge distribution.

We did not attempt to rigorously explore the sensitivity of the PNP model to alterations in the input parameters. As stated previously, the PNP model does not appear to be sensitive to changes in the assigned values for dielectric constant of the membrane and pore, but this insensitivity may be related to the ionic conditions and charge distributions used in our study. In some cases, the model did not appear to be very sensitive to rather substantial changes in charge distribution. This is illustrated in Fig. 13, A–C, where two different charge distribution models of the Cx26/Cx32*Cx26($NT_{1–11}$+CL) channel result in very similar I–V relations with the PNP model in the symmetric 150-mM salt case. The two charge distribution models differ only by the presence of an internal negative charge ($-0.5\ e$), which we propose to correspond to residue E41 in Cx32 (see above). However, the two charge distribution models can in principle be discriminated in other pairing configurations or by varying the ionic concentration parameter used in the PNP model. For example, the I–V relations obtained for the two different models of Cx32*Cx26 ($NT_{1–11}$+CL) differ somewhat when they are used to form homotypic channels (Fig. 13 D). Also, the I–V relations (and predicted reversal potential) of the two different heterotypic Cx26/Cx32*Cx26($NT_{1–11}$+CL) channels differ slightly when asymmetric salts (15 mM inside:150 mM outside) are used (Fig. 13 E). The incorporation of the negative charge shifts the reversal potential from −10 to 0 mV. Greater differences in the I–V relations are obtained with the PNP model in the symmetric salt case when the concentration of ions is reduced to 15 mM from 150 mM (Fig. 13 F). Although it is not clear whether the differences in the I–V relations shown in Fig. 13 can be resolved experimentally, it seems at least theoretically possible that the PNP model is able to discriminate among different charge distribution models when the model's input parameters are varied.

The results of our molecular studies in conjunction with PNP theory have enabled us to identify at least one internally consistent set of charge distributions that can explain the observed rectification of several hetero- and homotypic channels. This finding supports the view that charged amino acid residues in the NT and E1 domain of Cx32 and Cx26 are important molecular determinants of electrical rectification. The questions, if the charge distributions models derived here are unique and if the PNP model can provide a "unique" solution in all cases needs to be addressed further, but this aim is computationally and experimentally intensive and beyond the scope of the current paper.

Substate Rectification

We cannot legitimately apply the PNP model to explain the rectification observed in substates of Cx32 and Cx32*Cx26($NT_{1–11}$+CL) hemichannels as the available model considers the surface charge distribution of channels of right circular cylindrical geometry. While the changes in conformation associated with V_j gating to substates may not substantially change the magnitude of surface charge, it is likely that reductions in pore radius would increase the electrostatic effect of charges located in constricted regions. We illustrate this by considering the charge distribution models

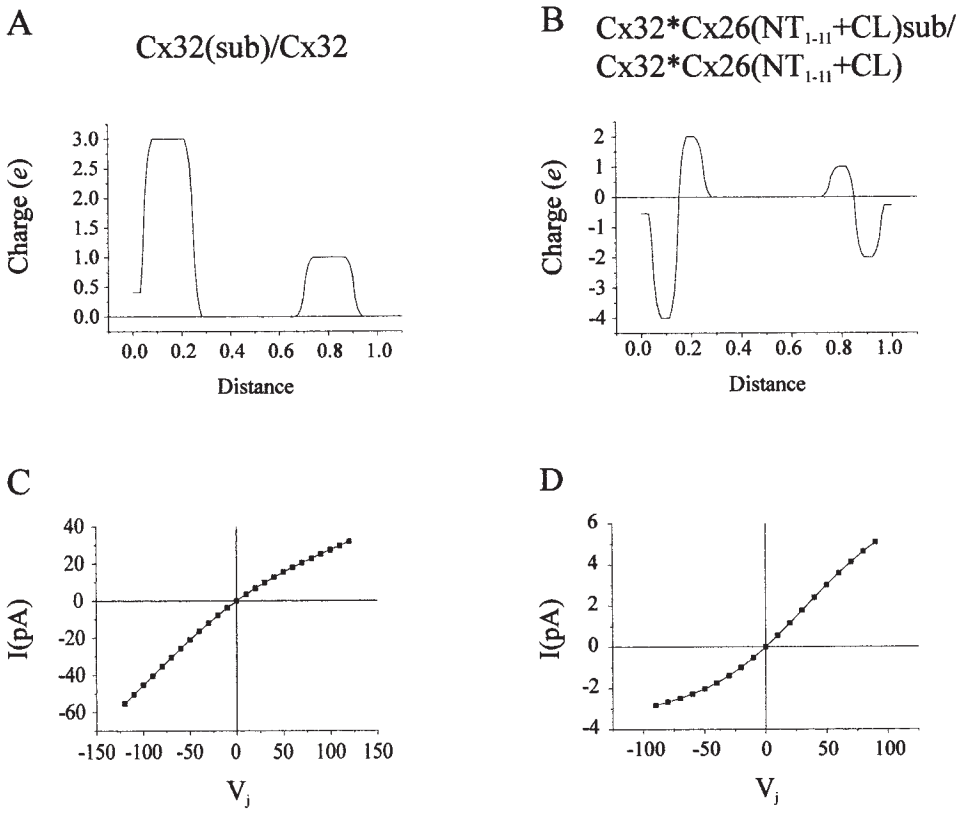

Figure 14. Charge distribution models and I–V relations obtained with the PNP model to illustrate the expected result of increasing the electrostatic effect of charged residues in one half of a gap junction channel. (A and C) A charge distribution model that may mimic the Cx32 substate leads to an I–V relation that resembles that of an observed Cx32 substate when used in the PNP model. The left side of the channel would be closed by the application of negative V_j. (B and D) A charge distribution model that may mimic the behavior of the Cx32*Cx26($NT_{1–11}$+CL) substate leads to an I–V relation that resembles that observed for the substate. The right side of the channel would be closed by the application of a negative V_j to the left side of the channel.

shown in Fig. 14. If one increases the magnitude of the external charges in the simple charge distribution models of Cx32 and Cx32*Cx26($NT_{1–11}$+CL) to mimic an increased electrostatic effect of these charges, then the I–V relations obtained rectify in the same direction as observed (compare Fig. 14, C and D, with Figs. 3 B and 7 E). When the Cx32 homotypic channel enters a substate in response to negative V_j, currents decrease as V_j becomes more positive (Fig. 14 C). In homotypic Cx32*Cx26($NT_{1–11}$+CL) channels, current increases as the cell containing the hemichannel rendering in a substate becomes positive (Fig. 14 D). Note that Cx32 and Cx32*Cx26($NT_{1–11}$+CL) hemichannels close for opposite polarities of transjunctional voltage. Nonner and Eisenberg (1998) have considered the problem of nonuniform channel geometry. A comparable approach may allow a more appropriate consideration of the observed substate rectification.

Rectification of Electrical Synapses

The results obtained from the application of the PNP model can provide a mechanistic explanation for the generation of steeply rectifying electrical synapses originally reported by Furshpan and Potter (1959). The model illustrates how the separation of fixed positive and negative charges across the junctional membrane could result in a steeply rectifying electrical synapse (Fig. 15). In this context, our results subsume the diode hypothesis (i.e., the formation of a p-n junction by the separation of fixed positive and negative charges) that was originally proposed by Furshpan and Potter (1959). The steep rectification attainable by p-n junctions was also demonstrated by Mauro (1962) and Finkelstein (1963) using Nernst-Plank equations with the electroneutrality condition.

Jaslove and Brink (1986) suggested that voltage-dependent gating may also contribute to the steepness of the rectification observed in the crayfish electrical synapse. They and Giaume et al. (1987) have postulated that the crayfish electrical synapse is asymmetric; i.e., composed of two different hemichannels, one of which contains a fast voltage-dependent gate. It is possible that both the crayfish and hatchetfish electrical synapses (Auerbach and Bennett, 1969) are formed by a heterotypic junction in which the steady state conductance–voltage relation of one hemichannel is shifted to smaller transjunctional potentials, comparable with the inferred steady state conductance–voltage relation of the Cx26D2N hemichannel in the heterotypic Cx32/Cx26D2N junction (Fig. 8 B). The open probability of such a channel would be close to zero at $V_j = 0$ and increase upon depolarization of the presynaptic cell. This model would explain the low conductance of electrical synapses when coupled neurons have (or are held at) similar resting membrane potentials (Giaume and Korn,

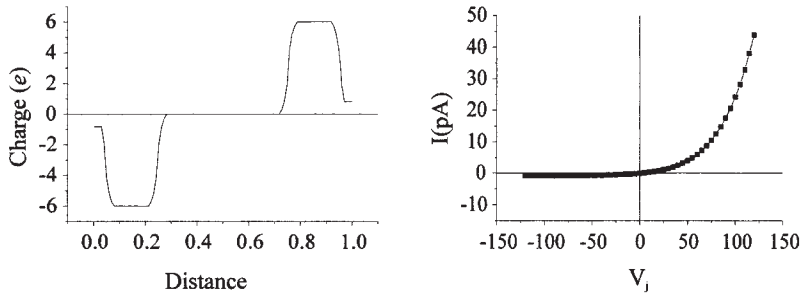

Figure 15. A charge distribution model and I–V relation obtained with the PNP model in symmetric 150 mM salt illustrating electrical rectification comparable in steepness to that reported for rectifying electrical synapses.

1985). Depolarization of the presynaptic cell (or hyperpolarization of the postsynaptic cell) would increase the open probability of this hemichannel, and increase junctional conductance. Hyperpolarization of the presynaptic cell (or depolarization of the postsynaptic cell) would favor the closed configuration. In this model, the presynaptic cell would contain a V_j gate like that of Cx32, which closes on relative negativity.

Voltage-dependent gating is unlikely to be the sole determinant of the electrical rectification observed in electrical synapses because steady state conductance at these synapses is reached very rapidly within 800 μs (Giaume et al., 1987). None of the cloned connexins that have been examined demonstrate sufficiently rapid kinetics. For example, Bukauskas et al. (1995b) reported that the mean time to reopen a closed Cx40 channel is 9.5 ms when the polarity of a transjunctional voltage step is reversed from +50 to −50 mV. But this is still much too slow to account for the properties of the crayfish electrical synapse. In preliminary studies, we have measured the mean time to reopen a closed Cx32 channel to be much slower, ~50–75 ms, when the polarity of a transjunctional voltage step is reversed from +100 to −100 mV (Oh, S., V.K. Verselis, and T.A. Bargiello, unpublished observations).

The rectification of gap junction open states and substates described in this study provides a mechanism that would allow for a nearly instantaneous increase in conductance in response to presynaptic depolarization. Electrodiffusive models (PNP theory and Nernst-Plank with electroneutrality assumption) predict steeply rectifying I–V relations for channels in which positive and negative charges are located at opposite ends of an intracellular channel (p-n junction). Thus, the steepness of the I–V relations attainable by p-n junctions can adequately explain the observed behavior of electrical synapses and obviates the need to invoke voltage gating. Recently, several fish connexins (O'Brien et al., 1996) as well as an unrelated family of invertebrate proteins encoding gap junctions have been cloned (Phelan et al., 1998), and it should soon be possible to identify the connexins that form rectifying electrical synapses and to precisely define the mechanism responsible for their steep rectification.

We thank Drs. A. Finkelstein, S. Slatin, P. Kienker, M. Colombini, D. Chen, and Dr. O. Andersen for helpful discussions and insights into the use of electrodiffusive models, Brady Trexler for compiling the PNP computer program, Dr. H.-S. Shin for providing the IRES vector, and Dr. P. Brink for providing the *Neuro-2a* cell line expressing Cx32*Cx26E1.

This work was supported by the National Institutes of Health grant GM46889. Michael Bennett is the Sylvia and Robert S. Olnick Professor of Neuroscience.

Submitted: 18 February 1999 Revised: 26 May 1999 Accepted: 18 June 1999

references

Auerbach, A.A., and M.V.L. Bennett. 1969. A rectifying synapses in the central nervous system of a vertebrate. *J. Gen. Physiol.* 53:211–237.

Barrio, L.C., T. Suchyna, T. Bargiello, L.X. Xu, R.S. Roginski, M.V. Bennett, and B.J. Nicholson. 1991. Gap junctions formed by connexins 26 and 32 alone and in combination are differently affected by applied voltage. *Proc. Natl. Acad. Sci. USA.* 88:8410–8414.

Becker, M.D., D.V. Greathouse, R.E. Koeppe, and O.S. Andersen. 1991. Amino acid sequence modulation of gramicidin channel function: effects of tryptophan-to-phenylalanine substitutions on the single-channel conductance and duration. *Biochemistry.* 30: 8330–8339.

Bennett, M.V.L., J.B. Rubin, T.A. Bargiello, and V.K. Verselis. 1993. Structure–function studies of voltage sensitivity of connexins, the family of gap junction forming proteins. 1993. *Jpn. J. Physiol.* 43: S301–S310.

Bukauskas, F.F., and R. Weingart. 1994. Voltage-dependent gating of single gap junction channels in an insect cell line. *Biophys. J.* 67:613–625.

Bukauskas, F.F., C. Elfgang, K. Willecke, and R. Weingart. 1995a. Heterotypic gap junction channels (connexin26-connexin32) violate the paradigm of unitary conductance. *Pflügers Arch.* 429: 870–872.

Bukauskas, F.F., C. Elfgang, K. Willecke, and R. Weingart. 1995b. Biophysical properties of gap junction channels formed by

mouse connexin40 in induced pairs of transfected HeLa cells. *Biophys. J.* 68:2289–2298.

Bukauskas, F.F., and C. Peracchia. 1997. Two distinct gating mechanisms in gap junction channels: CO2-sensitive and voltage sensitive. *Biophys. J.* 72:2137–2142.

Chen, D., and R. Eisenberg. 1993. Charges, currents and potentials in ionic channels of one conformation. *Biophys. J.* 64:1405–1421.

Chen, D., J. Lear, and B. Eisenberg. 1997. Permeation through an open channel: Poisson-Nernst-Plank theory of a synthetic ion channel. *Biophys. J.* 72:97–116.

Dorigo, A.E., D.G. Anderson, and D.D. Busath. 1999. Noncontact dipole effects on channel permeation. II. Trp conformations and dipole potentials in Gramicidin A. *Biophys. J.* 76:1897–1908.

Finkelstein, A. 1963. The role of time variant resistance and electromotive force in ionic systems related to cell membranes: the excitability properties of frog skin and toad bladder. Ph.D. Thesis, The Rockefeller University.

Furshpan, E.J., and D.D. Potter. 1959. Transmission at the giant motor synapse of the crayfish. *J. Physiol*. 145:289–325.

Giaume, C., and H. Korn. 1985. Junctional voltage-dependence at the crayfish rectifying synapse. *In* Gap Junctions. M.V.L. Bennett and D.C. Spray, editors. Cold Spring Harbor Laboratory, Cold Spring Harbor, NY. 367–379.

Giaume, C., R.T. Kado, and H. Korn. 1987. Voltage-clamp analysis of a crayfish rectifying synapse. *J. Physiol*. 386:91–112.

Hall, D.H., E.Gilat, and M.V.L. Bennett. 1985. Ultrastructure of the rectifying electrotonic synapses between giant fibers and pectoral fin adductor motorneurons in the hatchetfish. *J. Neurocytol*. 14: 825–834.

Jaslove, S.W., and P.R. Brink. 1986. The mechanism of rectification at the electrotonic motor giant synapse of the crayfish. *Nature.* 323:63–65.

Jongsma, H.J., R. Wilders, A.C.G. van Ginneken, and M.B. Rook. 1991. Modulatory effect of the transcellular electrical field on gap junction conductance. *In* Biophysics of Gap Junction Channels. C. Perrachia, editor. CRC Press, Baton Rouge, LA. 163–172.

Kumpf, R.A., and D.A. Dougherty. 1993. A mechanism for ion selectivity in potassium channels: computational studies of cation-π interactions. *Science.* 261:1708–1710.

Laio, A., and V. Torre. 1999. Physical origin of selectivity in ionic channels of biological membranes. *Biophys. J.* 76:129–146.

Mauro, A. 1962. Space charge regions in fixed charge membranes and the associated property of capacitance. *Biophys. J.* 2:179–198.

Mecozzi, S., A.P. West, Jr., and D.D Dougherty. 1996. Cation-π interactions in aromatics of biological and medicinal interest: electrostatic potential surfaces as a useful qualitative guide. *Proc. Natl. Acad. Sci. USA.* 93:10566–10571.

Moreno, A.P., M.B. Rook, G.I. Fishman, and D.C. Spray. 1994. Gap junction channels: distinct voltage-sensitive and -insensitive conductance states. *Biophys. J.* 67:113–119.

Neyton, J., and A. Trautman. 1985. Single channel currents of an intercellular junction. *Nature.* 317:331–335.

Nonner, W., and B. Eisenberg. 1998. Ion permeation and glutamate residues linked by Poisson-Nernst-Plank theory in L-type calcium channels. *Biophys. J.* 75:1287–1305.

O'Brien, J., M.R. Al-Ulbaidi, and H. Ripps. 1996. Connexin 35: a gap-junctional protein expressed preferentially in the skate retina. *Mol. Biol. Cell.* 7:233–243.

Oh, S., Y. Ri, M.V.L. Bennett, E.B. Trexler, V.K. Verselis, and T.A. Bargiello. 1997. Changes in permeability caused by connexin 32 mutations underlie X-linked Charcot-Marie-Tooth disease. *Neuron*. 19:927–938.

Phelan, P., L.A. Stebbings, R.A. Baines, J.P. Bacon, J.A. Davies, and C. Ford. 1998. *Drosophila* Shaking-B protein forms gap junctions in paired *Xenopus* oocytes. *Nature.* 391:181–184.

Rubin, J.B. 1992. Molecular analysis of gap junction voltage dependence. Ph.D. thesis. Albert Einstein College of Medicine, New York.

Rubin, J.B., V.K. Verselis, M.V.L. Bennett, and T.A. Bargiello. 1992a. Molecular analysis of voltage dependence of heterotypic gap junctions formed by connexins 26 and 32. *Biophys. J.* 62:183–195.

Rubin, J.B., V.K. Verselis, M.V.L. Bennett, and T.A. Bargiello. 1992b. A domain substitution procedure and its use to analyze voltage dependence of homotypic gap junctions formed by connexins 26 and 32. *Proc. Natl. Acad. Sci. USA.* 89:3820–3824.

Trexler, E.B., M.V.L. Bennett, T.A. Bargiello, and V.K Verselis. 1996. Voltage gating and permeation in a gap junction hemichannel. *Proc. Natl. Acad. Sci. USA.* 93:5836–5841.

Veenstra, R.D. 1996. Size and selectivity of gap junction channels formed from different connexins. *J. Bioenerg. Biomembr.* 28:327–337.

Verselis, V.K., C.S. Ginter, and T.A. Bargiello. 1994. Opposite voltage gating polarities of two closely related connexins. *Nature.* 368:348–351.